# VIBRATION-BASED STIFFNESS AND DAMPING MATRICES UPDATING OF A SANDWICH COMPOSITE BEAM

By

Eslie R. Castro Moura

A thesis submitted in partial fulfillment of the requirements for the degree of

MASTER OF SCIENCES

IN

MECHANICAL ENGINEERING

UNIVERSITY OF PUERTO RICO

MAYAGÜEZ CAMPUS

May 2004

Approved by:

_____     May 20 2004
Frederick A. Just, Ph. D.                         Date
President of Graduate Committee

_____     5/13/04
David Serrano, Sc. D.                             Date
Member of Graduate Committee

_____     5/20/04
Abdul Basir Shafiq, Ph. D.                        Date
Member of Graduate Committee

_____     May 20, 2004
Luis E. Suarez, Ph. D.                            Date
Representative of Graduate Studies

_____     5/21/04
Paul Sundaram, Ph. D.                             Date
Chairperson of Department

**Abstract**

This investigation seeks to develop a dynamic model capable of predicting the dynamic behavior of a sandwich composite beam. This work is based on the previous works of Lancaster, Pilkey and Ortiz. A vibration-based methodology is presented to calculate and update both the damping and stiffness matrices of the model. Initially a Finite Element Model (**FEM**) of the beam is developed. Along with this model, modal properties of the beam system are obtained from Frequency Response Functions (**FRF**). With this information, an iterative computational algorithm is used to identify the damping matrix of the system and update the stiffness matrix. These two updated matrices, along with the mass matrix obtained from the *FEM*, make up the analytical model of the structure. This analytical model is used to generate *FRF's*, which are in turn compared to their experimental counterparts.

Damage was induced in the beams and studied. The results showed that the analytical models could be adjusted to the damaged beams. The dynamic behavior of the beam system could be predicted with the analytical model. Therefore, the damping and stiffness matrices identified and updated by the algorithm adequately represent the structure's damping and stiffness characteristics.

**Resumen**

Esta investigación propone desarrollar un modelo dinámico capaz de predecir el comportamiento dinámico de una viga de material compuesto en capas. Este trabajo está basado en los trabajos anteriores de Lancaster, Pilkey y Ortiz. Se presenta una metodología, basada en ensayos de vibración, con el fin de calcular y actualizar las matrices de amortiguamiento y rigidez del modelo. Se desarrolla inicialmente un modelo de elemento finito de la viga. En conjunto con el modelo, las propiedades modales del sistema de viga se obtienen de las funciones de respuesta de frecuencias. Con esta información, se utiliza un algoritmo de iteración computacional para identificar la matriz de amortiguamiento del sistema y actualizar la matriz de rigidez. Estas dos matrices actualizadas, en conjunto con la matriz de masa obtenida por medio del método de elementos finitos, forman el modelo analítico de la estructura. Este modelo analítico es utilizado para generar funciones de respuestas de frecuencias, que a su vez se comparan con sus contrapartes experimentales.

Se indujo y estudio daño en las vigas. Los resultados demuestran que los modelos analíticos pueden ser ajustados adecuadamente a vigas con presencia de daño. El comportamiento dinámico del sistema de viga puede ser predicho por el modelo analítico. Esto nos confirma que las matrices obtenidas por el método presentado, las matrices de amortiguamiento y rigidez, pueden ser identificadas y actualizadas adecuadamente por el algoritmo y representan de manera fiel las características de amortiguamiento y rigidez del sistema.

**Acknowledgements**

First, I would like to express my thanks and gratitude to my advisor, Dr. Frederick Just. Thanks for the opportunity given to me to be part of this project. Also thanks for his guidance, support and encouragement during the course of completing this work. Thanks being a mentor and a friend. I would also like to thank doctors B. Shafiq and D. Serrano for being part of my graduate committee and for their input into this project.

Thanks also to all the graduate students working in the Dynamics Lab. for their support and the help provided. Special thanks to J. Jairo and J. Mesa for their support and friendship. Thanks to M. Ortiz for her disposition and her input with respect to the technical information and background used in this investigation.

I would also like to thank my family: my mother Ada and my father Rafael for their unconditional love and support. Thanks to my brother Rafi and his family for their encouragement. Thanks to my girl Jania for her friendship, love and support. Thanks to all my friends for taking me in for the last three years, giving me their friendship, encouragement and sometimes a place to stay. Last but not least I would like to thank God for giving me this opportunity and for being there when needed the most.

**Table of Contents**

**List of Tables**

**List of Figures**

**List of Symbols**

| | |
|---|---|
| $[Z(\omega)]$ | Dynamic stiffness matrix. |
| $[\alpha(\omega)]$ | Receptance matrix. |
| $[d(\omega)]$ | Difference vector. |
| *FRF* | Frequency Response Function. |
| *DOF* | Degree of Freedom. |
| $[M]$ | Mass matrix. |
| $[C]$ | Damping matrix. |
| $[C_0]$ | Initial damping matrix. |
| $[K]$ | Stiffness matrix. |
| $[I]$ | Identity matrix. |
| $\lambda_i$ | $i^{th}$ eigenvalue. |
| $\Lambda$ | Eigenvalue matrix. |
| $\varphi_i$ | $i^{th}$ eigenvector. |
| $\Phi$ | Eigenvector matrix. |
| *MAC* | Modal assurance criteria. |
| *UMPA* | Unified matrix polynomial approach. |
| *FEM* | Finite element model. |
| *IRS* | Improved reduced system. |
| *IIRS* | Iterated improved reduced system. |
| *q* | Left eigenvectors. |
| *r* | Right eigenvectors. |
| $[Q]$ | Left eigenvector matrix. |
| $[R]$ | Right eigenvector matrix. |
| $\omega$ | Driving frequency. |
| *m* | Mass coefficient. |
| *c* | Damping coefficient. |
| *k* | Stiffness coefficient. |
| $\ddot{x}, \dot{x}, x$ | State vectors, (acceleration, velocity, displacement). |
| $H(i\omega)$ | Complex transfer function. |

| | |
|---|---|
| $i, j$ | $\sqrt{-1}$ . |
| $\zeta$ | Modal damping ratio. |
| $fe^{i\omega t}$ | Harmonic input force. |
| $\boldsymbol{\Lambda_C}$ | Modal damping matrix. |
| $\boldsymbol{\Lambda_K}$ | Modal stiffness matrix. |
| $\boldsymbol{u_i}$ | Real mode shape vector. |
| $\psi$ | Complex eigenvector. |
| $\boldsymbol{\Psi}$ | Complex eigenvector matrix. |
| $\boldsymbol{T}$ | Transformation matrix. |
| $\boldsymbol{x_m}$ | Master coordinates. |
| $\boldsymbol{x_s}$ | Slave coordinates. |
| $\boldsymbol{P}, \boldsymbol{F}$ | Force. |
| $\boldsymbol{\delta}$ | Displacement, deformation. |
| $\overline{m}$ | Mass per unit length. |

**List of Appendixes**

**Chapter One:**

**Introduction**

Model updating is the process where an initial theoretical representation of the dynamical behavior of a structure can be refined, corrected or updated using experimental data acquired from tests performed on the actual structure. This area of research has attracted a lot of attention and acquired importance lately. The need for these updating procedures is due to the ever presence of errors associated with constructing a theoretical model of the structure. Another important aspect of model updating comes from the need for improved performance of engineering designs and the materials used in those designs.

Modeling real life structures can be a difficult and strenuous task. Structures may incorporate different elements. The variety of these elements and their interaction contributes to the structure's complexity. Certain modeling techniques enable engineers to understand complex systems by breaking them into smaller, simpler systems which can be easily studied. These smaller systems facilitate the task at hand while accurately portraying the larger, more complex system.

Damage detection is currently an area under extensive research. Obviously, the importance of damage detection is the added capability of a system to be diagnosed prior to the failure of such system. To accurately anticipate failure or damage of a design equates into more safe, efficient, and economical designs. Damage detection is a field that automatically benefits from model updating techniques. The scope of this study is to create a model that will enable a neural network to detect presence of damage on the structures.

The general procedure for damage detection is:

1. Perform a modal analysis on the undamaged structure,
2. Perform the same analysis on the damaged structure and
3. Relate the changes exhibited by the undamaged and the damaged structure to the damage to which the structure was subjected.

Extensive research has been conducted in this field, (references [1-6]) with little attention paid to composite materials. These materials have become very popular and

provide the engineer with an alternative to traditional materials used in certain application. Their attractiveness resides in that they can practically be tailored for a specific applications. An example of their benefits is the fact that they can provide high stiffness, high strength and exhibit little weight. These characteristics make them attractive for a wide range of applications, including the fields of aerospace, marine, automotives, general transportation and structures, to name a few.

The specific composite category dealt with in this investigation is a sandwich composite. A sandwich composite structure is a special form of a laminated composite comprising a combination of different materials that are bonded to each other so as to utilize the properties of each separate component to the structural advantage of the whole assembly. Typically a sandwich composite consists of three main parts; two thin, stiff and strong faces separated by a thick, light and weaker core. The faces are adhesively bonded to the core to obtain a load transfer between the components. The faces of the composite give the material its strength and stiffness while the core provides absorption of impacts by load transfer between adjacent cells within the core. The primary advantage of a sandwich composite is very high stiffness-to-weight ratio and high bending strength-to-weight ratio. The sandwich enhances the flexural rigidity of the structure without adding substantial weight. Sandwich composites also have great impact resistance, wear resistance, fatigue resistance and high energy absorbing capabilities.

Diagnostics of structural health, using vibration response, is of great importance and has immense potential in areas such as aerospace, mechanical and civil engineering. It is important to study composite materials and their behavior under vibrations in order to extent their usage and applications for structural purposes. The study of sandwich composites and their dynamic behavior will provide us with the necessary tools to accurately predict changes and damage in the structure. If we are able to accurately predict changes in the structural behavior of a system, the reliability of the system increases due to the fact that adjustments are made to the structure and structural failure can be prevented.

In this research we will update a finite element model using vibration response. This research will apply specifically to sandwich composites, an area that has not been

extensively studied using vibration response methods. The model updating will be done utilizing an iterative method (Lancaster [7-8] & Pilkey [9-10]) that will establish a damping matrix which will in turn be used to determine the stiffness matrix directly. The procedure will be performed for both the undamaged and damaged cases. Frequency responses functions (*FRF's*) will be generated to confirm the behavior of our model with that of the experimental case. The procedure will make use of the mass properties of the system and the modal data (damping ratios, eigenvalues and mode shapes) which is extracted from the experimental Frequency Response Functions (*FRF's*).

**Chapter Two:**

**Literature Review**

Extensive research has been done in the area of damage detection. Different types of techniques are available that address this purpose. In trying to limit the scope concerning the topic of this thesis, only works concerning frequency response methods will be reviewed.

Tran et al. [5] utilized changes in stiffness in order to characterize the damage and detect its presence. A simple cantilever thin plate was used in this study. Here frequency response function (*FRF*) data was used to find the structural damage. The method rests on the assumption that the damages affected mainly the stiffness of the specimen, while mass and damping properties remained largely unchanged.

This article was based on the observation that the dynamic stiffness matrix $[Z(\omega)]$ and *FRF* receptance matrix $[\alpha(\omega)]$ of a dynamic structure are orthogonal to each other,

$$[Z(\omega)][\alpha(\omega)] = ([K] - \omega^2[M])[\alpha(\omega)] = [I]. \tag{1.1}$$

Damage was identified by locating the coordinates where stiffness changes took place. A receptance difference vector, $[d(\omega)]$, was assembled and indicated which coordinates displayed changes in stiffness due to damage. These vectors were plotted against the frequencies of interest in a 3D Damage Location Plot. The approach used in this investigation, regarding the incompleteness of *FRF* data, was to simply eliminate the rows and columns corresponding to the unmeasured degrees of freedom (*DOF*). A finite element analysis of an undamaged homogeneous steel plate was conducted. The mass, *M*, and stiffness, *K*, matrices were generated. A crack was introduced in the model by reducing the Young's Modulus by 30% in a selected element. The mass and stiffness matrices were again generated with the simulated damage. Comparing the *FRF* data for both models did not detect the damage. However the 3D Plot was able to identify the damage location.

Capecchi et al. [11] studied three different geometries in which damage was represented by a linear decrement of stiffness. Here, the stiffness was unchanged throughout the structure except in a few damaged locations. The cases investigated were

a simply supported beam, a three span continuous beam and a ten-story shear frame. The method used an optimization approach with objective function $\underline{l}(\alpha)$ given by:

$$\underline{l}(\alpha) = \sum_i \left[ \det\left( \frac{\nabla \lambda_i}{H_\alpha^i} \right) \right]^2 \qquad (1.2)$$

where $\lambda_i$ is the set of $(n+1)$ eigenvalues and $\boldsymbol{H}_\alpha^i$ is the eigen-function matrix. The damage was located where the objective function was minimized or equal to 0. Here, only frequencies are assumed as modal characteristics and the damaged identification is based on the minimization of the objective function that accounts for the discrepancies between analytical and experimental quantities.

Kosmatka et al. [1] detected damages with a non destructive methodology. The procedure made use of measured modes and frequencies along with residual forces and a weighted sensitivity analysis to estimate mass and stiffness variation. Determination of the residual forces and the weighted sensitivity analysis required the use of a model correlated to the experimental baseline data from the undamaged structural state, which was used as the reference state.

This method used measured data to locate potentially damaged regions, using the residual modal force vectors, and conducted a sensitivity analysis to account for variations in mass and/or stiffness where damage was represented by a stiffness reduction. Other advantages of the method is that it accounts for variations in the system's mass, stiffness and center of mass locations, perturbations of natural frequencies and modal vectors, and confidence factors for structural parameters and instrumentation error.

Other techniques employ the use of damage indices as damage indicators. Kim et al. [2] developed vibration based algorithms to locate and estimate the severity of damage in structures. A series of algorithms were developed to improve the accuracy of the method. An equation for the damage index, $\boldsymbol{B_j}$, was derived. It was defined as the fraction of modal energy of the $\boldsymbol{i_{th}}$ mode and the $\boldsymbol{j_{th}}$ member. These methods give information regarding the location and the severity of damage from changes in the mode

shapes of the structure and use stiffness changes in order to detect damage. Damping characteristics were not taken in consideration.

Ratcliffe et al. [4] used non destructive vibration based techniques for locating delamination damage in a composite beam. Here the method makes use of the displacement eigenvector and converts it into a curvature mode shape. A damage detection index locates the delamination, irrespective of its position along the beam or depth within the beam.

This technique was demonstrated with a finite element model of a composite beam, where the damage was represented by a relaxation of the connectivity between elements at a desired position. The gapped smoothing damage detection method was validated experimentally.

Wang et al. [6] developed a detection algorithm that uses *FRF* data measured prior and posterior to structural damage. From this data, a damage vector was extracted indication both magnitude and location of damage. In order to account for model incompleteness an iterative version of the algorithm was introduced.

Baruch et al. [12-13] proposed a direct method for stiffness updating. The method utilizes modal data in order to update the stiffness matrix of the model. The mode shapes are corrected to satisfy the orthogonality requirement. The method includes the treatment of weighted orthonormal conditions and number of mode shapes less than the number of *DOF* of the structure. The paper also presents a variation of this method, which deals with the manipulation of the flexibility matrix. This corrected flexibility matrix incorporates the corrected mode shapes and the measured frequencies.

Ewins [14] presents a review of the terminology involved in model adjusting or model updating. He outlines different model updating algorithms currently available, with a discussion of each algorithms' functionality, advantages and disadvantages. He concludes with general comments on how to correctly set up for model updating and some of the limitations of the process.

Aiad et al. [15] presents a procedure to improve analytical models from measured complex modes. The mass and stiffness matrices are updated from experimental data. The example under study is a clamped plate. The mass and stiffness matrices are

corrected by using different conditions in order to make the matrices meet the orthogonality requirement. A modal assurance criteria (***MAC***) comparison is shown to confirm the effectiveness of the model.

Imregun et al. [16] outlines the basic formulation of an *FRF* based updating method. Several solution strategies are presented. Simulated data is used to provide a better picture of the uniqueness of the model, the effectiveness of the updating method and the influence of noisy data and incomplete experimental data in the model. Stability of the method and convergence of the model is also studied in some detail. Finally the basic algorithm is extended to include complex *FRF* data and deal with proportional damped systems.

Friswell and Lees [17] present a paper concerned with the resonance frequency of damped structures. They define the resonance frequency as the local maximum of the response. This frequency is not necessarily the undamped or damped natural frequency. The maximum may exhibit a shift due to the influence of neighboring modes and their influence upon the response. Special attention is paid to rotating structures, where the definition of these resonance frequencies or critical speeds change depending on which degree of freedom is being considered.

Allemang and Brown [18] examine different approaches to handling modal data and reformulating modal parameter estimation algorithms. A matrix polynomial approach is used to unify the presentation of the different algorithms currently available. This unified matrix polynomial approach (***UMPA***) allows a discussion of the similarities and differences between the different methods. Depending upon the situation and quantity of experimental data available, the method to be used varies, with some methods more appropriate than others. Methods such as least squares, total least squares, double least squares and singular value decomposition take advantage of redundant measurement data. Eigenvalue and singular value decomposition transformations are used to effectively reduce the size of the resulting eigenvalue-eigenvectors problem.

Friswell, Inman and Pilkey [19] propose a method to update the damping and stiffness matrices simultaneously. The mass matrix is assumed correct, while the other matrices are updated reproducing the measured modal data. The method minimizes the

change in damping and stiffness, with the measured data as a constraint. The approach was demonstrated using a simulated example, producing reasonable results. The algorithm does not guarantee that the updated matrices are positive definite and the preservation of the original finite element model's connectivity.

Lancaster [7-8] presents a methodology to invert lambda matrices. The paper first considers the inversion of a general matrix polynomial defined by:

$$D^{(l)}(\lambda) \equiv \left(A_0 \lambda^l + A_1 \lambda^{l-1} + \cdots + A_{l-1} \lambda + A_l\right). \tag{1.3}$$

Applying this notation to a dynamic system, where the superscript $l = 2$, the matrices for the polynomial terms become $A_0 = M$, $A_1 = C$ and $A_2 = K$. This equation represents a dynamic system with a mass, damping and stiffness matrices.

$$D^{(2)}(\lambda) \equiv \left(M\lambda^2 + C\lambda + K\right) \tag{1.4}$$

From this, Lancaster presents two theorems that will help to manipulate this expression. The first theorem expresses that if $M$ and $K$ are symmetric and $M$ is nonsingular then

$$\begin{aligned}
(M\lambda + K)q &= 0 \\
(M^T \lambda + K^T)r &= 0
\end{aligned} \tag{1.5}$$

where $q$ and $r$ are the right and left eigenvectors of the system.

This expressions can be normalized in a way such that

$$\begin{aligned}
R^T M Q &= I \\
R^T K Q &= -\Lambda
\end{aligned}, \tag{1.6}$$

which leads to

$$(M\lambda + K)^{-1} = Q(I\lambda - \Lambda)^{-1} R^T. \tag{1.7}$$

The second theorem states that if $M$ is nonsingular and $D^{(2)}(\lambda)$ has a degeneracy equal to the multiplicity of $\lambda_i$ for $i = 1, 2, 3, \ldots, 2n$, then the eigenvectors can be normalized such that

$$\lambda^{0,1}\left[D^2(\lambda)\right]^{-1} = Q\Lambda^{0,1}(I\lambda - \Lambda)^{-1} R^T \tag{1.8}$$

and

$$\lambda^2\left[D^2(\lambda)\right]^{-1} = Q\Lambda^2(I\lambda - \Lambda)^{-1} R^T + M^{-1}. \tag{1.9}$$

For the previous equations Q and R are matrices populated by the left and right eigenvectors of the system. By realizing that the left and right eigenvectors are identical and that they occur in complex conjugate pairs, a normalizing condition can be established as

$$\phi_i^T \left( 2M\lambda_i + C_0 \right) \phi_i = 1 \qquad (1.10)$$

and a definition for the damping matrix can be given as

$$C = -M \left( \Phi \Lambda^2 \Phi^T + \overline{\Phi \Lambda^2 \Phi^T} \right) M . \qquad (1.11)$$

Lancaster also defines the stiffness matrix as

$$K^{-1} = -\Phi \Lambda^{-1} \Phi^T - \overline{\Phi \Lambda^{-1} \Phi^T} . \qquad (1.12)$$

The methodology is applicable to underdamped systems, where the eigenvalues of the system occur in complex conjugate pairs.

Pilkey [8-9] introduced an iterative method with damage detection capabilities. This technique is robust and is able to identify the damping matrix of a structure. The algorithm considers viscous damping, dealing in turn with complex eigenvectors and eigenvalues. The method is based on work by Lancaster [21]. The calculation of the damping matrix requires a known finite element model and eigen data. The paper also compares different methods for model reduction and updating.

Ortiz [3] used Pilkey's methods to study its applicability to a sandwich composite beam. The method effectively combined the *FRF* data with *FEM* data (both mass and stiffness matrices were generated with finite element techniques), and results were able to generate a damping matrix that characterized the system. Models were established and compared against experimental *FRF* data. It was concluded that the method could produce a mathematical model for sandwich composite that predicted actual beam behavior.

**Chapter Three:**

**Theoretical Background**

Various techniques are available for finite element updating. Two ways, discrete parameter models and continuous models, delineate the manner in which systems can be described. In discrete parameter system models, the system is an assembly of rigid body masses and deformable, massless elements. Another way in which a system can be described is to assume that the mass and deformation is distributed throughout the system, this is a distributed or continuous parameter system. A continuous model will be a better choice for describing a system, but in practice this approach is not always possible. Sometimes the equations of motion of the system are difficult or impossible to solve in a closed form.

The approach used in this investigation is the discrete parameter approach. Here some assumptions were made to facilitate the study of the system. Mass, stiffness and damping properties of the system are assumed to be invariant with respect to time and deformations in the structure are small and follow a linear stress-strain relationship. Because of this linear behavior, the structure is said to be linear and the principle of superposition can be used in the analysis of the structure. This principle can be described as follows: if the application of a force $F_A$ causes the system to react by deforming with a deformation $\delta_A$ and another force, $F_B$, is applied independently causing an arbitrary deformation $\delta_B$ then the application of both forces simultaneously will cause the system to react by deforming by an amount $\delta_T = \delta_A + \delta_B$.

To ensure that our structure behaves linearly, a slender beam serves as our test structure. Depth and height of the beam are small compared to the length dimension. This being said, we can assume that the plane section of the beam will remain plane during the process of vibration. For the analysis of our structure it is quite reasonable to assume linear behavior of the system, hence the principle of superposition is applicable. Because of linearity we can also assume the composite has an equivalent modulus of elasticity, a physical property that will dictate the magnitude of the components of the stiffness matrix.

In order to obtain an analytical model of the system, the structure is subjected to experimental modal analysis techniques. This modal testing is conducted with the purpose of obtaining the modal parameters of the structure, such as natural frequencies, eigenvalues and eigenvectors. The modal analysis, in addition to the finite element model of the structure, can be used to generate an analytical model whose behavior is comparable to the actual or experimental behavior of the structure.

Mathematical Modeling

A beam is structural member whose primary function is to support transverse loading. Being a continuous system, the beam's mass and stiffness are distributed evenly along the length of the longitudinal axis. In order to properly describe the behavior of the beam, a discrete system will be used. The beam is divided into equal elements having uniform physical properties. With this in mind, two different approaches can be used to define the model: a lumped mass approach and a consistent mass approach.

For a model based on the lumped mass approach, the displacements of all points within the element are equivalent to the displacement of the element's centroid and the model's accuracy increases as the number of elements increase. A typical discrete model using three masses is depicted in Figure 3.1.
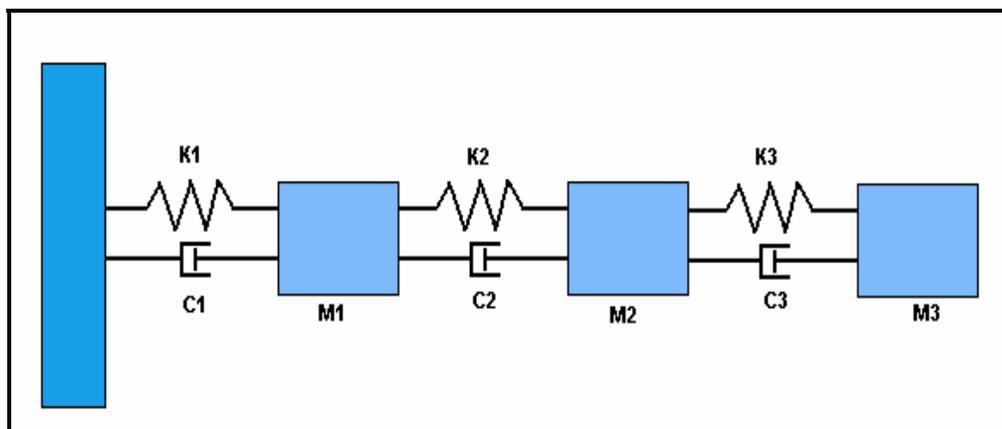


**Figure 3.1: Discrete Model with Three Degrees of Freedom.**

Here, the dynamic behavior of the system can be described using Newton's second law. Each mass element is assigned a unique coordinate system to describe its

motion: displacement, velocity and acceleration. Structural and dissipative forces are represented by spring and dashpot elements respectively. Application of the above procedure yields a set of coupled equations in the form of:

$$M\ddot{x} + C\dot{x} + Kx = F \tag{3.1}$$

where $M$ is the mass matrix, $C$ is the damping matrix and $K$ is the stiffness matrix of the system.

The definition of each matrix is given below as:

$$M = \begin{bmatrix} m_1 & 0 & 0 \\ 0 & m_2 & 0 \\ 0 & 0 & m_3 \end{bmatrix} \qquad C = \begin{bmatrix} c_1 + c_2 & -c_2 & 0 \\ -c_2 & c_2 + c_3 & -c_3 \\ 0 & -c_3 & c_3 \end{bmatrix}$$

$$K = \begin{bmatrix} k_1 + k_2 & -k_2 & 0 \\ -k_2 & k_2 + k_3 & -k_3 \\ 0 & -k_3 & k_3 \end{bmatrix}$$

The consistent mass approach is based on beam theory. The simplest and best known model of these theories is the Euler Bernoulli Beam Theory, commonly referred to as classical beam theory. In order to use this theory, certain assumptions are made. The beam is assumed to have plane symmetry, plane sections originally normal to the longitudinal axis of the beam remain plane and normal to the deformed longitudinal axis upon bending. Also the internal strain energy of the beam member accounts only for bending moment deformations.

In this theory, the transverse deflection of the beam $w$ is governed by the differential equation:

$$\frac{d^2}{dx^2}\left(EI\frac{d^2w}{dx^2}\right) = f(x) \qquad \text{for } 0 < x < L \tag{3.2}$$

Because we have four boundary conditions per element, a polynomial interpolation function of the form $w(x) = c_1 x^3 + c_2 x^2 + c_3 x + c_4$ is chosen to describe the deflection of the beam element. In order to evaluate the constants of the previous expression, the boundary conditions for each element must be met which are the displacement and slope at each node of the element given by:

$$w(0) = w_1 \qquad \frac{dw}{dx}(0) = w_2$$
$$w(l) = w_3 \qquad \frac{dw}{dx}(l) = w_4$$

(3.3)

From these expressions, the approximate displacement for the element can be expressed as:

$$w(x) = \left[1 - 3\frac{x^2}{l^2} + 2\frac{x^3}{l^3}\right]w_1 + l\left[\frac{x}{l} - 2\frac{x^2}{l^2} + 3\frac{x^3}{l^3}\right]w_2 + \left[3\frac{x^2}{l^2} - 2\frac{x^3}{l^3}\right]w_3 + l\left[-\frac{x^2}{l^2} + \frac{x^3}{l^3}\right]w_4$$

(3.4)

where $l$ is the element's length.

The shape function vector can be expressed as

$$\varphi = \begin{bmatrix} 1 - 3\dfrac{x^2}{l^2} + 2\dfrac{x^3}{l^3} \\[2mm] l\left(\dfrac{x}{l} - 2\dfrac{x^2}{l^2} + 3\dfrac{x^3}{l^3}\right) \\[2mm] 3\dfrac{x^2}{l^2} - 2\dfrac{x^3}{l^3} \\[2mm] l\left(-\dfrac{x^2}{l^2} + \dfrac{x^3}{l^3}\right) \end{bmatrix}$$

(3.5)

Using this vector and the definition of kinetic energy, the mass matrix for an element of the beam can be defined as

$$M_{ij} = \overline{m} \int_0^l \varphi_i \varphi_j \, dx$$

(3.6)

where $\overline{m}$ is mass per unit length.

Similarly the stiffness matrix can be defined as

$$K_{ij} = EI \int_0^l \frac{d^2\varphi_i}{dx^2} \frac{d^2\varphi_j}{dx^2} \, dx$$

(3.7)

Using these expressions the mass and stiffness matrix for each element are obtained as:

$$M = \frac{\overline{ml}}{420} \begin{bmatrix} 156 & 22l & 54 & -13l \\ 22l & 4l^2 & 13l & -3l^2 \\ 54 & 13l & 156 & -22l \\ -13l & -3l^2 & -22l & 4l^2 \end{bmatrix} \tag{3.8}$$

and

$$K = \frac{EI}{l^3} \begin{bmatrix} 12 & 6l & -12 & 6l \\ 6l & 4l^2 & -6l & 2l^2 \\ -12 & -6l & 12 & -6l \\ 6l & 2l^2 & -6l & 4l^2 \end{bmatrix} \tag{3.9}$$

where **EI** is the modulus of rigidity of the beam.

The model that will be developed consists of four elements with five nodes. Global matrices representing the system's mass and stiffness are 10 by 10 symmetric matrices.

Modal Analysis

Modal analysis refers to the process of identifying the system's modal characteristics such as natural frequencies, mode shapes and damping ratios. This information is gathered via vibration experiments, specifically by generating Frequency Response Functions (*FRF*) of the system. The Frequency Response plots the magnitude of the transfer function against the frequency at which the system is excited. Figure 3.2 shows a typical Frequency Response Function. The natural frequencies can be identified by looking at the different peaks of the graph.
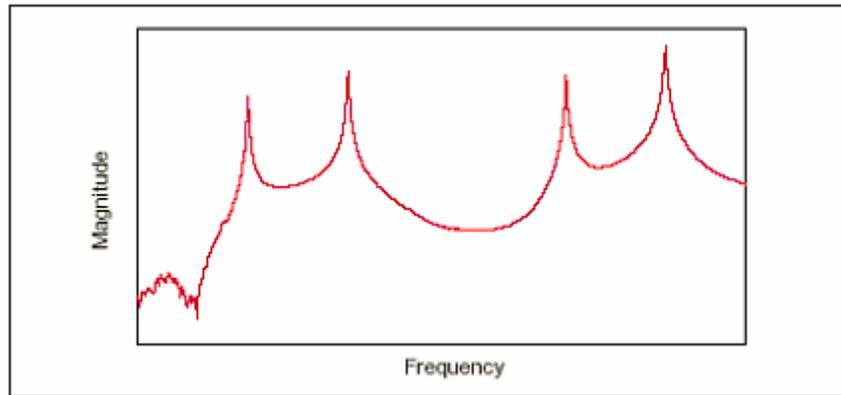
**Figure 3.2: Frequency Response Function Plot.**

The information obtained from the modal analysis, in conjunction with the finite element model developed previously, will be used to accomplish the task at hand, updating the finite element model. The updated model will be compared with the experimental *FRF* for the purpose of validating the reduced model's ability to predict dynamic behavior. Modal analysis can be summarized in three steps: extraction of modal properties from the *FRF* plot, identification of mode shapes and vibration modes, and structural model updating.

For the analysis of the Frequency Response the Single Degree of Freedom Method (***SDOF***) was used. In this method the Frequency Response Function is sectioned off into frequency ranges bracketing each peak. Each peak is analyzed independently and is seen as the response of a single degree of freedom system. This implies that in the vicinity on the resonant peak the Response Function is dominated by a specific single mode. To properly identify a resonant peak two characteristics must be present: the magnitude of the Frequency Response must be at a maximum and a phase shift of approximately 90 degrees must occur.

A Frequency Response Function can be defined as the ratio of the output to the input under steady state conditions when the excitation is purely harmonic. Consider the single degree of freedom equation:

$$m\ddot{x} + c\dot{x} + kx = y(t) \tag{3.10}$$

in which $x$ is the system's output and $y(t)$ is the input forcing function. Assuming a solution of the form $y(t) = e^{i\omega t}$, the output of the system may be expressed as $x = H(i\omega)e^{i\omega t}$, where $H(i\omega)$ is a complex function. Substitution into equation 3.10 yields

$$H(\omega) = \frac{1}{(k - m\omega^2) + (c\omega)i}. \tag{3.11}$$

Here $m$, $c$, $k$ and $\omega$ represent the mass, damping, stiffness and driving frequency respectively.

An analogous statement could be made with respect to our *MDOF* system. By examining equation 3.1, the system can be defined by the matrix equation

$$M\ddot{x} + C\dot{x} + Kx = F \tag{3.12}$$

where $M$ is the mass matrix, $C$ is the damping matrix and $K$ is the stiffness matrix of the system. Taking the Laplace transform of the system and applying a unit impulse forcing vector yields the following: $(Ms^2 + Cs + K)X(s) = \{1\}$. By manipulating this expression, we can easily arrive to an equation similar to equation 3.11. To transfer the equation to the frequency domain, let $s = j\omega$. The matrices in equation 3.12 are symmetric, real and positive definite.

The largest value of the *FRF* magnitude occurs at resonance, when the driving frequency is near the natural frequency $\omega = \sqrt{k/m}$. This corresponds to a peak in the *FRF* plot. At this condition, large displacements and stresses are developed in the system. Here lies the importance of vibration analysis for structures.

In this analysis, a composite beam is vibrated and measurements are taken at each element. The data collected is used to generate the *FRF* plots for the beam. A shaker is used to impart the motion into the system, via a signal generator. The shaker vibrates randomly within the frequency range of interest. The input signal is measured by an accelerometer and the output by a laser vibrometer conditioned through a dynamic signal analyzer (see Figure 3.3). The signals are then processed by the software, generating the *FRF* of the specimen.
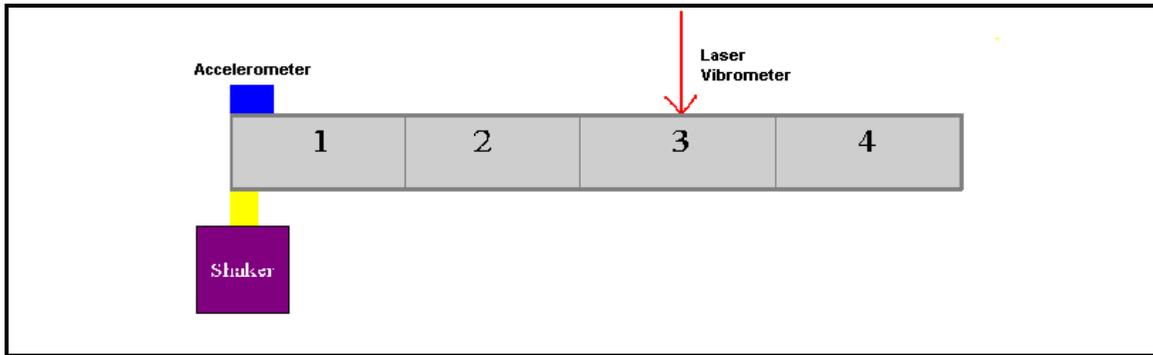
**Figure 3.3: Experimental Setup.**

From the generated *FRF* plots, modal parameters are extracted. The modal parameters of interest are the values for the maximum value of the transfer function, the modal damping ratio and the natural frequency of the system. The *FRF* plots were analyzed using the *SDOF* method discussed previously. Various methods are available for the extraction of the modal parameters for each of the *SDOF* systems. The method to be employed in this investigation will be described in the following section. For each element of the finite element model, four *SDOF* Transfer Functions are examined, each function corresponding to the first four natural frequencies of that particular element.

Nyquist Plots

A Nyquist plot, also known as the circle fitting method, is a systematic method for obtaining modal parameters from Response Functions. Basically a Nyquist diagram plots the real part of the complex transfer function versus the imaginary part. This is done for a specific frequency range, around a resonance peak of the general *FRF* (*SDOF* method). For the *SDOF*, in the vicinity of resonance, the resulting graph resembles the figure of a circle, hence the name circle fitting technique.

To construct a Nyquist plot first the frequency range of interest is divided into equally spaced segments and a complex response is associated with each of the frequencies. Then the plot is generated using the real and imaginary parts of the response. The magnitude of the response is equal to the distance from the response point to the origin. From this concept we could say that resonance occurs at a frequency whose

corresponding point in the Nyquist circle is farthest from the origin. If the point corresponding to the resonant condition was not included in the diagram, the natural frequency is the point lying halfway the longest arc between two adjacent points (see Figure 3.4).
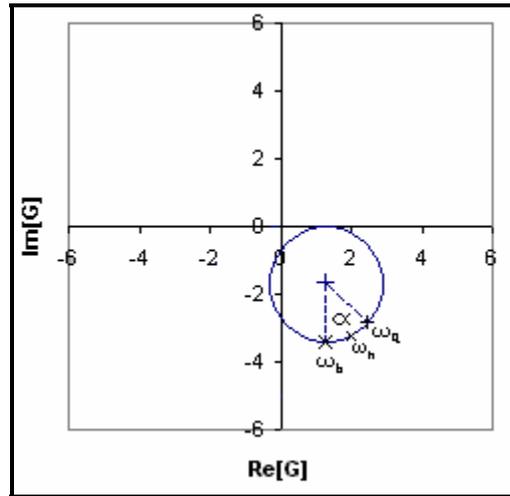


**Figure 3.4: Nyquist Plot.**

The adjacent points forming the largest arc of the circle correspond to the frequencies $\omega_a$ and $\omega_b$. The natural frequency, $\omega_n$, can be estimated as the frequency corresponding to point halfway through the arc. Using the coordinates of points $\omega_a$, $\omega_b$ and the center of the circle, the natural frequency and the angle $\alpha$ are calculated. After obtaining the modal frequency, the modal damping ratio can be approximated with the relation:

$$\zeta = \frac{\omega_b^2 - \omega_a^2}{2\omega_n \left[ \omega_a \tan\left(\frac{\alpha}{2}\right) + \omega_b \tan\left(\frac{\alpha}{2}\right) \right]} \tag{3.13}$$

The last piece of modal information that is needed is the mode shape for each individual natural frequency. The procedure to extract the mode shapes of the system is taken from Inman [20]. The theory presented here will explain how to obtain real mode shapes from the experimental data (damping ratio, frequency response and natural frequencies).

Determining the mode shapes of a multiple degree of freedom system involves the measurement of several *FRF*. First a *FRF* matrix, or receptance matrix, is established. Consider the system described by

$$M\ddot{x} + C\dot{x} + Kx = fe^{j\omega t} \tag{3.14}$$

where $fe^{j\omega t}$ is harmonic input force in complex form. Assuming a harmonic solution to the system, $x(t) = ue^{j\omega t}$, and combining with equation 3.14 yields

$$\left(K - \omega^2 M + j\omega C\right)u = f \tag{3.15}$$

From the equation above we can define the receptance matrix, *α(ω)*, as the ratio of displacement to force, which yields

$$\alpha(\omega) = \left(K - \omega^2 M + j\omega C\right)^{-1} \tag{3.16}$$

The receptance matrix can be further analyzed through the modal coordinates transformations. From this transformations modal stiffness and modal damping matrices can be written in diagonal form as

$$\Lambda_K = diagonal\left[\omega_i^2\right] = P^T M^{-\frac{1}{2}} K M^{-\frac{1}{2}} P \tag{3.17}$$

$$\Lambda_C = diagonal\left[2\zeta_i \omega_i\right] = P^T M^{-\frac{1}{2}} C M^{-\frac{1}{2}} P \tag{3.18}$$

where *P* is the matrix of normalized eigenvectors of the matrix $M^{-\frac{1}{2}} K M^{-\frac{1}{2}}$. Rearranging these expressions for *K* and *C* and substituting into equation 3.16 yield

$$
\begin{aligned}
\alpha(\omega) &= \left[ M^{\frac{1}{2}} P\left(\Lambda_K - \omega^2 I + j\omega\Lambda_C\right) P^T M^{\frac{1}{2}} \right]^{-1} \\
&= \left[ S\left(\Lambda_K - \omega^2 I + j\omega\Lambda_C\right) S^T \right]^{-1} \\
&= \left[ S\, diagonal\left[\omega_i^2 - \omega^2 + 2\zeta_i \omega_i \omega j\right] S^T \right]^{-1}
\end{aligned}
\tag{3.19}
$$

where $S = M^{\frac{1}{2}} P$ consisting of column vectors $u_i$.

From matrix theory *(AB)⁻¹ = B⁻¹A⁻¹*, so

$$\alpha(\omega) = S^{-T}\, diagonal\left[\frac{1}{\omega_i^2 - \omega^2 + 2\zeta_i \omega_i \omega j}\right] S^{-1} \tag{3.20}$$

By realizing that, in equation 3.20, the columns of $S^T$ are the mode shape vectors of the undamped system, denoted $u_i$, equation 3.20 can be written as the summation

$$\alpha(\omega) = \sum_{i=1}^{n} \frac{\left[u_i u_i^T\right]}{\left(\omega_i^2 - \omega^2\right) + \left(2\zeta_i \omega_i \omega\right)j} \tag{3.21}$$

where $u_i u_i^T$ is the outer product of two $n \times 1$ mode shape vectors.

The element $\alpha_{sr}$ of the receptance matrix corresponds to the frequency transfer function between the measured response, $u_s$, at node **s** caused by the input force $f_r$ at node **r**, when all other inputs are zero (refer to Figure 3.5). Therefore the element can be defined as

$$\alpha_{sr}(\omega) = \sum_{i=1}^{n} \frac{\left|u_i u_i^T\right|_{sr}}{\left(\omega_i^2 - \omega^2\right) + \left(2\zeta_i \omega_i \omega\right)j} \tag{3.22}$$

Each element of $\alpha(\omega)$ is a transfer function defined by

$$\frac{u_s}{f_r} = \left[\alpha(\omega)\right]_{sr} = H_{sr}(\omega) \tag{3.23}$$

where $H(\omega)$ is the transfer function.

If the peaks of the system are well spaced, the summation of equation 3.22 is dominated by the term corresponding to that particular frequency. This is equivalent to saying that $\omega = \omega_i$ and substituting into equation 3.22, yields

$$\left|\alpha_{sr}(\omega)\right| = \frac{\left|u_i u_i^T\right|_{sr}}{2\zeta_i \omega_i^2} \tag{3.24}$$

which, with equation 3.23, can be rearranged as

$$\left|u_i u_i^T\right|_{sr} = \left|2\zeta_i \omega_i^2\right| \left|H_{sr}(\omega_i)\right| \tag{3.25}$$

This derivation holds for proportionally damped systems with underdamped, widely spaced modes and the procedure gives an approximation of the modes of the structure by relating the measures damping ratio, the measured natural frequency and the measured transfer function. Also, this procedure gives an approximation of the magnitude of eigenvector matrix. The sign of this vector can be obtained from the phase plot of the transfer function. At resonance the phase should +90° or -90°. If the phase corresponding to that element of the mode vector is +90°, the element is positive.

Otherwise the element is assigned a negative value. Next we will go step by step through an example of this methodology.

A Cantilever Beam Example

Consider the cantilever beam shown in Figure 3.5 in which three experimental *FRF* plots have been obtained.
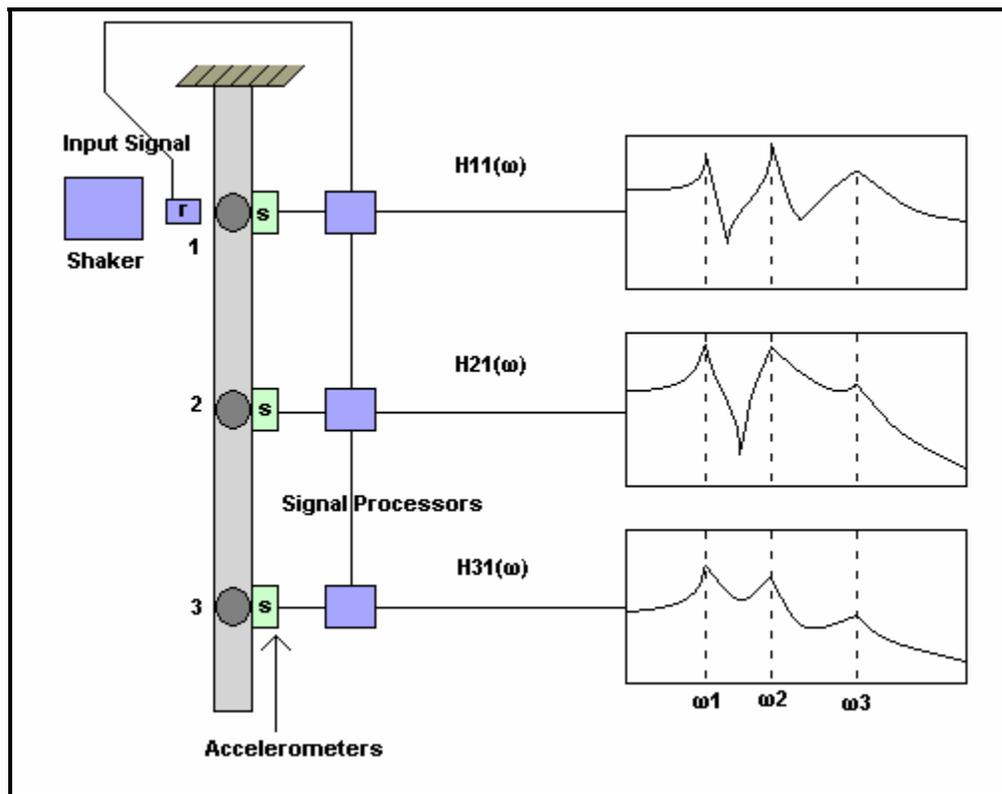


**Figure 3.5: Mode Shape Acquisition.**

From these *FRF* plots, the natural frequencies and the damping ratios are obtained. In addition, we can obtain the values for the magnitude and phase of the transfer function. In order to continue refer to the values given in Tables 3.1 and 3.2.

**Table 3.1: Natural Frequencies and Damping Ratios**

| Natural Frequencies and Damping Ratios | | |
|---|---|---|
| Mode Index (i) | $\omega_i$ (rads/s) | $\zeta_i$ |
| 1 | 10 | 0.01 |
| 2 | 20 | 0.01 |
| 3 | 32 | 0.05 |

**Table 3.2: Data for Mode Shape Extraction.**

| Frequency Response Data | | | | | | |
|---|---|---|---|---|---|---|
| Position | $\omega_1$(rads/s) | | $\omega_2$(rads/s) | | $\omega_3$(rads/s) | |
| Index (i) | $|H_i(\omega)|$ | Phase(º) | $|H_i(\omega)|$ | Phase(º) | $|H_i(\omega)|$ | Phase(º) |
| 11 | 0.423 | -90 | 0.68 | -90 | 0.14 | -90 |
| 21 | 0.917 | -90 | 0.77 | -90 | 0.12 | +90 |
| 31 | 2.316 | -90 | 2.05 | +90 | 0.70 | -90 |

Using equation 3.25 with the corresponding values of $\zeta_1$, $\omega_1$, $H_{11}(\omega_1)$, $H_{21}(\omega_1)$, $H_{31}(\omega_1)$, the first row of matrix $|u_1u_1^T|$ is determined to be:

$$|u_1u_1^T|_{11}=0.846 \qquad\qquad |u_1u_1^T|_{21}=1.834 \qquad\qquad |u_1u_1^T|_{31}=4.633$$

The mode shape vector $u_1$ is defined as $u_1 = [a_1\ a_2\ a_3]^T$, then

$$u_1u_1^T = \begin{bmatrix} a_1^2 & a_1a_2 & a_1a_3 \\ a_2a_1 & a_2^2 & a_2a_3 \\ a_3a_1 & a_3a_2 & a_3^2 \end{bmatrix} \qquad (3.26)$$

thus $a_1^2=0.846$, $a_1a_2=1.834$ and $a_1a_3=4.633$, yielding

$$u_1 = \begin{bmatrix} a_1 \\ a_2 \\ a_3 \end{bmatrix} = \begin{bmatrix} -0.920 \\ -1.993 \\ -5.036 \end{bmatrix}.$$

Note that the elements of $\mathbf{u_1}$ are all negative because the corresponding phase angles for the magnitudes of the *FRF* around the first natural frequency are all negative. Similarly the next two mode shapes can be approximated as:

$$u_2 = \begin{bmatrix} -2.332 \\ -2.642 \\ 7.033 \end{bmatrix} \qquad u_3 = \begin{bmatrix} -3.7863 \\ 3.2453 \\ -18.931 \end{bmatrix}$$

The procedure explained above is used to obtain real mode shapes of a structure. The mode shapes needed for completion of our study can be complex. The procedure to obtain these mode shapes is similar to the method explained above with a few slight modifications. Expression 3.22 can be expressed as

$$[H(\omega)] = \sum_{j=r}^{2n} \frac{\lambda_j}{i\omega - \lambda_j} \Psi_j \Psi_j^T = [\Psi]\left[\frac{\lambda_j}{i\omega - \lambda_j}\right][\Psi]^T \tag{3.27}$$

where $\lambda_j$ is the complex natural frequency and $\Psi_j$ is the mode shape corresponding to that frequency. By using this notation, the response of the system can be given in the form of

$$u = [H(\omega)]fe^{i\omega t}. \tag{3.28}$$

Substitution of $\lambda_j = -\alpha_j + i\omega_{dj}$ in equation 3.27 yields

$$H_{sr}(\omega_j) \approx \frac{-\alpha_j + i\omega_{dj}}{\alpha_j} \Psi_{rj} \Psi_{sj} \tag{3.29}$$

where the subscript $s$ is the node corresponding to the output measurement and $r$ is the location of the node where the excitation is applied. The term $\omega_d$ is the damped natural frequency of the specimen. With

$$\alpha_j = \zeta_j\omega_j \text{ and } \omega_{dj} = \omega_j\sqrt{1-\zeta_j^2}. \tag{3.30}$$

By using the aforementioned relationship, equation 3.29 can be expressed as

$$H_{sr}(\omega) \approx \left(-1 + \frac{i\sqrt{1-\zeta_j^2}}{\zeta_j}\right)\Psi_{rj}\Psi_{sj}. \tag{3.31}$$

As $\zeta_j$ becomes smaller, expression 3.31 can be simplified as

$$H_{sr}(\omega) \approx \left(\frac{-\zeta_j + i}{\zeta_j}\right)\Psi_{rj}\Psi_{sj}. \tag{3.32}$$

For the case when $s = r$ the term of the mode shape can be calculated using

$$\Psi_{si} = \left( \frac{\zeta_j}{-\zeta_j + i} H_{ss} \right)^{\frac{1}{2}} .$$  (3.33)

Other terms can be found once this first term is calculated.

$$\Psi_{ri} = \left( \frac{\zeta_j}{-\zeta_j + i} \frac{H_{rs}}{\Psi_{sj}} \right)$$  (3.34)

For the experimental cases the mode shapes were acquired using the Star Modal software. The software performs the necessary computations to extract the mode shapes, natural frequencies and damping ratios.


## Model Incompatibility and Model Reduction


As discussed before, the Finite Element Model (*FEM*) was used to model a cantilever beam system. There are two degrees of freedom associated with each node of the element model. One degree of freedom corresponds to the translational displacement of the node; the other degree of freedom corresponds to the rotational degree of freedom. This resulted in 10 by 10 matrices for the mass and stiffness associated with the system. From the boundary conditions of the system, there are no displacements at node 1; therefore the model could be reduced to an 8 by 8 system.

In practice, only translational degrees of freedom can be accurately measured. These translational degrees of freedom were used to obtain the modal data for the system. Due to this limitation, the *FEM* has to be reduced to make it compatible with the available degrees of freedom measured, thus mass and stiffness matrices have to be transformed, so a model dependant only upon the translational degrees of freedom can be established.

To accomplish this, there are several available methods. One of the oldest and most popular methods is the Guyan Reduction or static reduction [21]. In this reduction the inertia terms associated with the discarded degrees of freedom are neglected. This reduction is exact at zero frequency, but when applied to a dynamic system the reduction

may lack accuracy. The Improved Reduced System (***IRS***) [22] is a modified method based on the Guyan Reduction. In this method, an extra term is added to the static reduction transformation to make some allowances for the inertia forces of the discarded degrees of freedom. The Improved Reduced System has been extended to use a dynamic reduction transformation, instead of the static transformation, as the basic transformation and thus making the process an iterative process with proven convergence (Friswell et. al., [23]). This method is known as the Iterated Improved Reduced System (***IIRS***).

In the *IIRS* procedure, the process of reducing the model starts with the partitioning of the mass and stiffness matrices. The partitions are done because of the reordering of the degrees of freedom of the system. The degrees of freedom of the system are classified into master and slave degrees of freedom. For the current purpose, a master degree of freedom, denoted by the subscript ***m***, corresponds to a measurable degree of freedom. A slave degree of freedom, subscript ***s***, corresponds to an immeasurable degree of freedom. Assuming that no forces are applied to the slave coordinates; the system can be described as

$$\begin{bmatrix} M_{mm} & M_{ms} \\ M_{sm} & M_{ss} \end{bmatrix} \begin{Bmatrix} \ddot{x}_m \\ \ddot{x}_s \end{Bmatrix} + \begin{bmatrix} K_{mm} & K_{ms} \\ K_{sm} & K_{ss} \end{bmatrix} \begin{Bmatrix} x_m \\ x_s \end{Bmatrix} = \begin{Bmatrix} f_m \\ 0 \end{Bmatrix} \tag{3.35}$$

where the mass and stiffness matrices appear partitioned according the relationship with the master and slave degrees of freedom.

By neglecting the inertia terms corresponding to slave coordinates, the static transformation (***T_s***) between the full state vector and the master coordinates can be defined as

$$\begin{Bmatrix} x_m \\ x_s \end{Bmatrix} = \begin{bmatrix} I \\ -K_{ss}^{-1} K_{sm} \end{bmatrix} x_m = T_s x_m \tag{3.36}$$

The reduced mass and stiffness matrices are

$$M_R = T_s^T M T_s \qquad K_R = T_s^T K T_s \tag{3.37}$$

In order to account for the inertia terms, a second term is added to the static reduction, ***T_s***, yielding the transformation for the Improved Reduced System, ***T_IRS***

$$T_{IRS} = T_s + S M T_s M_R^{-1} K_R \tag{3.38}$$

where

$$S = \begin{bmatrix} 0 & 0 \\ 0 & K_{ss}^{-1} \end{bmatrix} \tag{3.39}$$

The reduced mass and stiffness matrices for the *IRS* are

$$M_{IRS} = T_{IRS}^T M T_{IRS} \qquad K_{IRS} = T_{IRS}^T K T_{IRS} \tag{3.40}$$

The Iterated Improved Reduced System iterates the transformation matrix defined in equation 3.36. The iteration scheme is as follows. Assume an initial matrix of the form

$$T_{i+1} = \begin{bmatrix} I \\ t_{i+1} \end{bmatrix} \tag{3.41}$$

where $t_{i+1}$ is given by

$$t_{i+1} = t_s + K_{ss}^{-1}\begin{bmatrix} M_{sm} & M_{ss} \end{bmatrix} T_i M_{Ri}^{-1} K_{Ri} \tag{3.42}$$

and the initial transformation is the static transformation given by

$$t_0 = t_s = -K_{ss}^{-1} K_{sm} \tag{3.43}$$

The mass and stiffness reduced matrices of the i$^{th}$ iteration are

$$M_{Ri} = T_i^T M T_i \qquad K_{Ri} = T_i^T K T_i \tag{3.44}$$

The transformation matrix converges and the final reduced system is obtained from equations 3.41, 3.42 and 3.44.

The reduced model obtained from the reduction processes will be used, in conjunction with the modal properties and parameters, to properly identify a damping matrix and update the stiffness matrix suitable for the reduced model. The model obtained will be used to generate **FRF**, properly describing the beams' dynamic behavior.

**Chapter Four:**

**Methodology**

This chapter presents a description of the methods and materials used in this investigation. The methodology describes all the required analysis, intermediate steps and results needed to successfully accomplish the task of updating the stiffness matrix for the composite beams under study. Most of the methods described in this chapter are based in the theory presented in Chapter Three.

The beams studied in this investigation were layered composite beams. These beams were manufactured with facesheets consisting of two carbon fiber sheets and a foam filled honeycomb core. The frequency response function (*FRF*) of each beam is studied in order to extract certain modal characteristics. These characteristics are used to create a finite element model describing the dynamic behavior of the beams. Each beam is also subjected to damage in order to identify this damage from the *FRF's* and the finite element model. Changes in the characteristics of the *FEM*, the damping and stiffness matrices of the model, should also account for the changes due to the damage present in the beam. These *FEM's* are used to generate *FRF's* that can be used for damage detection through the use of different methods, for example the training of a neural network capable of distinguishing changes in *FRF's* from different damage scenarios (varying size and location of changes).

Once the physical properties of the beams were obtained (dimensions, equivalent modulus of elasticity, equivalent density, etc.), the theoretical natural frequencies were calculated. Experimental data was analyzed for both the undamaged and damaged cases with the help of MATLAB, SigLab and Star Modal software. Analysis routines were coded in the MATLAB program; that were based on the theory presented in Chapter Three. From the experimental *FRF* plots, the damping ratio, the natural frequency and the complex transfer function were identified. This information was used to calculate the eigenvalues and eigenvectors for each beam structure, with the Star Modal software. The mass and stiffness matrices were generated using finite element techniques. In order to make the finite element model compatible with the experimental process, the matrices

were reduced to a four degree of freedom system by a MATLAB code based on the *IIRS* methodology.

With the *FEM* matrices and the modal information, the damping and stiffness matrices of the system were identified and updated.  This was done through a MATLAB algorithm based on the theory presented by Lancaster [7-8] and Pilkey [9-10].   The updated model (mass, damping and stiffness matrices) *FRF* plots were regenerated for each system and compared with the experimental *FRF* plots to examine their adequacy in predicting dynamic system behavior.

Beam Properties and Dimensions

The physical information required from each beam was its dimensions, its mass and the modulus of elasticity.  As mentioned previously, three composite beams made out of carbon fiber and foam-filled honeycomb were available.  These three beams will be referred to as Beams 5, 6 and 8.  The mass of each beam was obtained by weighing.

The beams' modulus of rigidity (the product of the modulus of elasticity and the moment of inertia, *EI*) can be calculated through various methods.  For example, using the equations for natural frequency for cantilever beams described by Blevins [24], we can obtain an equivalent rigidity for the beams.  Another method is the use of the formula for layered composites, which defines the modulus as

$$EI = \sum_k 2E_k b \int_{d_k}^{d_{k+1}} y^2 dy = \frac{2b}{3} \sum_k E_k \left( d_{k+1}^3 - d_k^3 \right)$$

(4.1)

where $E_k$ is the modulus of elasticity of each layer, $b$ is the width of the beam, and $d_k$ is the distance from the neutral axis of the cross-section of the beam to the interface between the $k$ and the $k+1$ layer.  This formula requires the prior knowledge of the modulus for the material that makes up the beam.  Some materials used in the composite beams are low grade materials and the technical information needed, $E$, was not available.

Since the beams were long and slender, the calculation of the modulus for the composite beams was done experimentally.  Using the equation for the deflection of a

cantilever beam under static loading an equivalent modulus could be determined. The deflection of a beam depends upon its mechanical properties of and its dimensions. For a cantilever beam, as shown in Figure 4.1, the deflection of the beam is described by

$$\delta = \frac{Px^2}{6EI}(3a - x) \qquad (4.2)$$

where $a$ is the distance from the fixed end of the beam to the point where the load is placed and $x$ is the distance from the fixed end to the point where the displacement is being measured. Rearranging this equation and defining the slope $m$ as the ratio of the load to the deflection of the beam yields

$$EI = \frac{mx^2}{6}(3a - x) \qquad (4.3)$$

where $EI$ is the equivalent modulus of rigidity of the beam.
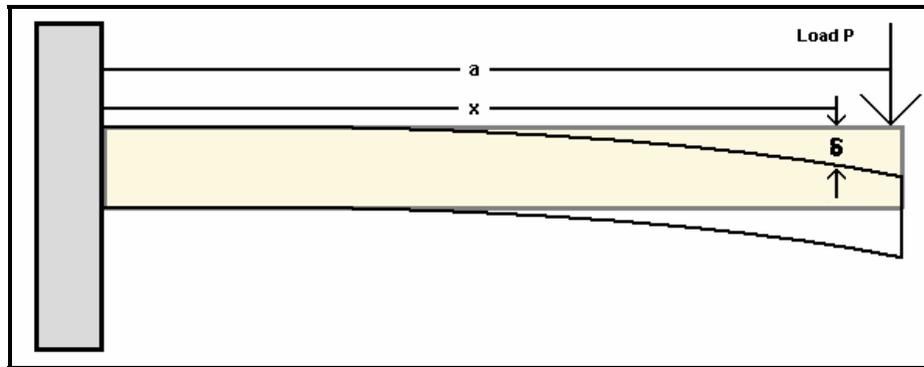


**Figure 4.1: Cantilever Beam with Concentrated Load Applied at the End.**

If a series of loads are applied to the beams and the correspondent deflection is measured, a load vs. deflection graph can be obtained. From this graph, the slope of the curve and an equivalent modulus of rigidity can be calculated using equation 4.3.

Experiments were performed on the three composite beams and each beam was subjected to a series of loads. Here the deflection for each load was measured and a graph of the load versus deflection was constructed. In addition, the slope of the best fit data line was also determined. With each correlation of the data, an R-squared value is determined using equation 4.4.

$$R^2 = 1 - \frac{\sum \left( Y_j - \hat{Y}_j \right)^2}{\left( \sum Y_j^2 \right) - \frac{\left( \sum Y_j \right)^2}{n}} \qquad (4.4)$$

These values reveal how closely the estimated values of the curve fit correspond to the actual data. The closer the R-squared value is to unity the better the fit. The resulting R-squared values for the correlations were close to 0.999, indicating that the use of equation 4.3 is acceptable. Figures 4.2, 4.3 and 4.4 graph the experimental result with their corresponding fit equation.

**Deflection of Bar 5**

$y = 341.64x + 0.0054$

$R^2 = 0.9992$

Load (N) vs. Deflection (m)
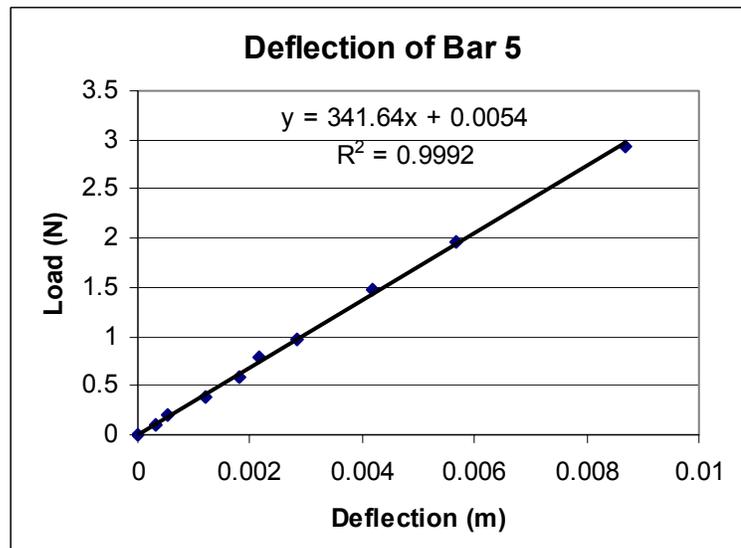
**Figure 4.2: Deflection vs. Load Curve for Beam 5.**
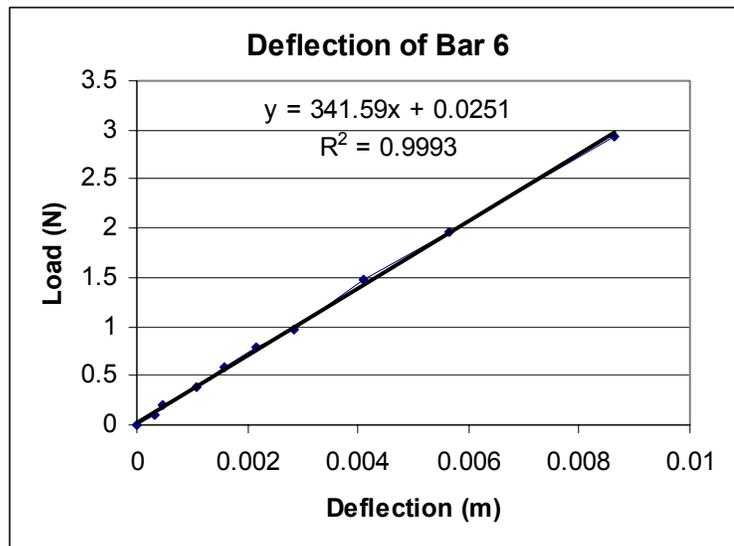
**Figure 4.3: Deflection vs. Load Curve for Beam 6.**
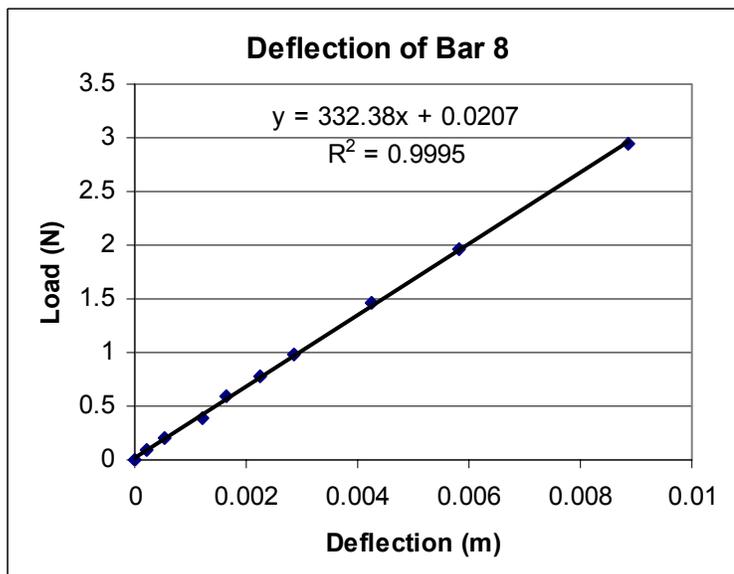


**Figure 4.4: Deflection vs. Load Curve for Beam 8.**

The beam properties mass and modulus of rigidity are summarized in Table 4.1. The average beam length was 1.219 meters with an average width of 5.1 centimeters and an average thickness of 7.264 millimeters.

**Table 4.1: Physical Properties for the Beams**

| Beam Property | Beam 5 | Beam 6 | Beam 8 |
|---|---|---|---|
| Mass (kg) | 0.15792 | 0.15723 | 0.15505 |
| Modulus *EI* (Nm$^2$) | 22.674 | 22.671 | 22.059 |

<u>Theoretical Natural Frequencies</u>

Using the physical and mechanical properties for each of the beams, the first four natural frequencies were calculated. The equation used for these calculations are outlined in Tse, Morse and Hinkle [25] and the natural frequencies are defined by:

$$f_n = \frac{(\beta l_n)^2}{2\pi l^2}\sqrt{\frac{EI}{\overline{m}}} \qquad (4.5)$$

where $\beta l_n$ is a parameter that depends on the mode of the natural frequency and the boundary condition of the beam, $l$ is the length of the beam and $\overline{m}$ is the mass per unit length of the beam. The values of $\beta l_n$ for the first four modes are given by

$$\beta l_n = \begin{Bmatrix} 1.8751 \\ 4.6941 \\ 7.8547 \\ 10.9955 \end{Bmatrix}.$$

Since the beams were supported as shown in Figure 4.1, the length is 0.6095 meters.

The theoretical natural frequencies and the experimental natural frequencies for the undamaged case of the beams are shown in the following table.

**Table 4.2: Theoretical and Experimental Natural Frequencies.**

| Natural Frequency (Hz) | Beam 5 | | Beam 6 | | Beam 8 | |
|---|---|---|---|---|---|---|
| | Theo. | Exp. | Theo. | Exp. | Theo. | Exp. |
| **Mode 1** | 19.932 | 2 1.536 | 19.971 | 2 1.403 | 19.838 | 2 1.480 |
| **Mode 2** | 124.912 | 129.721 | 125.155 | 131.074 | 124.32 | 131.935 |
| **Mode 3** | 349.758 | 346.148 | 350.439 | 348.208 | 3 48.10 | 350.004 |
| **Mode 4** | 685.386 | 634.078 | 686.721 | 636.725 | 682.138 | 639.451 |

The maximum error between the theoretical and experimental natural frequencies was 8.1%.

Damage Scenarios

One of the purposes of this investigation is to have an updated model for a specific specimen and explored the feasibility of this model to accurately indicate the presence of damage. This updated model will in turn serve as input for a neural network that will be capable of distinguishing between undamaged and damaged specimens. The neural network is capable of learning from these models and their *FRF's* to determine the amount of damage present and its location. A comparison is established between the property matrices (stiffness and damping matrices) of a specimen. Each test specimen is subjected to the experimental process twice. First the properties are obtained for an undamaged specimen. Secondly, damaged is induced in the same specimen and then the properties are calculated. The two scenarios for each specimen are compared in order to identify damage presence within the structure.

Damage in the beams consisted of a slit across the top face of the carbon fiber sheet. The slit was made with a vertical milling machine. The depth of the cut is between 0.2 and 0.3 mm. The location for the slit varies. Beam 5 and 6 have a slit located a quarter of the length from the fixed end of the beam. In beam 8 the damage is

located halfway of the beam. Refer to Figure 4.5 for a damage location diagram for the beams.
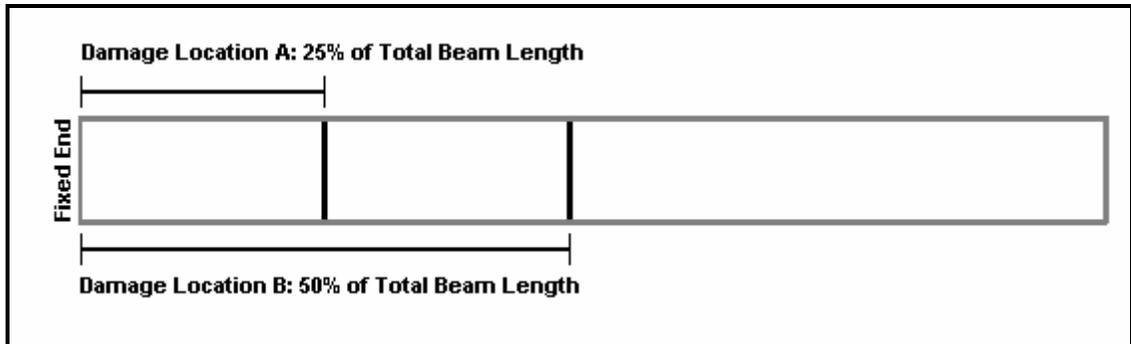


**Figure 4.5: Damage Locations for Experimental Specimens: Top View.**

As explained previously, each beam was vibrated twice. First the measurements were taken in the absence of damage. Then damage was induced in the beam and a second set of measurements were taken. The beams were divided into four elements as in Figure 3.3. The beams were vibrated with an electromagnetic shaker. The shaker received a random vibration signal, imparting the motion to the beam. This input signal was conditioned through the computer, with the help of MATLAB and SigLab software and hardware. Measurements of the signal were taken with two devices. The input signal's measurement was taken with an accelerometer. The output signal was measured with a laser vibrometer, which was integrated electronically using the SigLab dynamic signal analyzer. This measurement corresponds to the displacement of the beam at each segment of the beam. The natural frequencies and damping ratios corresponding to the different segments of the beams were obtained and averaged using Star Modal.

Tables 4.3 and 4.4 detail the average natural frequencies and damping ratios for each test specimen. Table 4.3 contains the data corresponding to the undamaged beams and Table 4.4 contains the data for the damaged beams.

**Table 4.3: Natural Frequencies and Damping Ratios for Undamaged Beams.**

| Modal Properties | Beam 5 | Beam 6 | Beam 8 |
|---|---|---|---|
| Natural Frequency (Hz) | | | |
| $\omega_1$ | 21.536 | 21.4032 | 21.481 |
| $\omega_2$ | 129.721 | 131.074 | 131.935 |
| $\omega_3$ | 346.148 | 348.208 | 350.004 |
| $\omega_4$ | 634.078 | 636.7249 | 639.451 |
| Damping Ratio | | | |
| $\zeta_1$ | 0.001623 | 0.002093 | 0.002095 |
| $\zeta_2$ | 0.002481 | 0.002181 | 0.002164 |
| $\zeta_3$ | 0.003105 | 0.003065 | 0.002990 |
| $\zeta_4$ | 0.004210 | 0.004123 | 0.004077 |

**Table 4.4: Natural Frequencies and Damping Ratios for Damaged Beams.**

| Modal Properties | Beam 5 | Beam 6 | Beam 8 |
|---|---|---|---|
| Natural Frequency (Hz) | | | |
| $\omega_1$ | 21.193 | 21.208 | 21.473 |
| $\omega_2$ | 129.807 | 131.112 | 131.520 |
| $\omega_3$ | 345.922 | 346.412 | 350.644 |
| $\omega_4$ | 633.829 | 634.805 | 638.880 |
| Damping Ratio | | | |
| $\zeta_1$ | 0.002203 | 0.001763 | 0.001785 |
| $\zeta_2$ | 0.002318 | 0.002178 | 0.002191 |
| $\zeta_3$ | 0.003126 | 0.003131 | 0.003041 |
| $\zeta_4$ | 0.004206 | 0.004148 | 0.004114 |

Eigen-Properties

The eigenvalues and eigenvectors of each of the beams were obtained using the Star Modal software.  The analysis of the experimental data was done by curve fitting the *FRF* measurements and the mode shapes were extracted using a technique similar to the one presented in the previous chapter.  The information obtained is presented in the following tables.

**Table 4.5: Eigen-Properties for Undamaged Beam 5.**

| Eigenvalues | | | |
|---|---|---|---|
| $1^{st}$ Eigenvalue | $2^{nd}$ Eigenvalue | $3^{rd}$ Eigenvalue | $4^{th}$ Eigenvalue |
| -0.21962 + 135.31i | -2.0222 + 815.06i | -6.7531 + 2174.9i | -16.773 + 3984i |
| **Eigenvectors** | | | |
| $1^{st}$ Mode Shape | $2^{nd}$ Mode Shape | $3^{rd}$ Mode Shape | $4^{th}$ Mode Shape |
| 0.7197 + 15.031i | 0.0731 + 33.579i | 0.0925 + 36.427i | 0.3706 + 23.085i |
| 2.354 + 52.28i | 1.1425 + 56.193i | 0.1178 - 1.4019i | -0.3356 - 25.017i |
| -0.1203 + 95.412i | 0.0523 + 9.2943i | -0.0526 - 27.285i | 0.2536 + 22.85i |
| 3.0486 + 149.24i | 0.0599 - 76.822i | 0.5682 + 46.136i | -0.2999 - 32.242i |

**Table 4.6: Eigen-Properties for Damaged Beam 5.**

| Eigenvalues | | | |
|---|---|---|---|
| $1^{st}$ Eigenvalue | $2^{nd}$ Eigenvalue | $3^{rd}$ Eigenvalue | $4^{th}$ Eigenvalue |
| -0.29335 + 133.16i | -1.8906 + 815.6i | -6.7943 + 2173.5i | -16.75 + 3982.4i |
| **Eigenvectors** | | | |
| $1^{st}$ Mode Shape | $2^{nd}$ Mode Shape | $3^{rd}$ Mode Shape | $4^{th}$ Mode Shape |
| -0.349 + 13.803i | -0.519 + 36.564i | 0.2071 + 38.378i | 0.3561 + 23.921i |
| 0.4715 + 47.678i | -0.3207 + 60.795i | -0.1685 - 1.5597i | -0.34 - 25.792i |
| 5.0074 + 88.622i | 0.0988 + 9.74i | -0.2057 - 28.143i | 0.3007 + 23.792i |
| 2.6287 + 130.71i | 0.8543 - 82.416i | 0.3855 + 48.034i | -0.4007 - 33.65i |

**Table 4.7: Eigen-Properties for Undamaged Beam 6.**

| Eigenvalues | | | |
|---|---|---|---|
| 1$^{st}$ Eigenvalue | 2$^{nd}$ Eigenvalue | 3$^{rd}$ Eigenvalue | 4$^{th}$ Eigenvalue |
| -0.28147 + 134.48i | -1.7962 + 823.56i | -6.7058 + 2187.8i | -16.495 + 4000.6i |
| Eigenvectors | | | |
| 1$^{st}$ Mode Shape | 2$^{nd}$ Mode Shape | 3$^{rd}$ Mode Shape | 4$^{th}$ Mode Shape |
| 0.003 + 13.599i | 0.3809 + 37.778i | 0.3332 + 38.81i | 0.394 + 24.31i |
| 1.0685 + 42.943i | -0.1866 + 59.731i | -0.1584 - 1.6813i | -0.4013 - 26.218i |
| 0.9647 + 84.901i | 0.0827 + 8.3652i | -0.2214 - 27.9i | 0.4277 + 24.382i |
| 3.7767 + 122.6i | -0.0374 - 82.044i | 0.3596 + 49.629i | -0.5219 - 36.563i |

**Table 4.8: Eigen-Properties for Damaged Beam 6.**

| Eigenvalues | | | |
|---|---|---|---|
| 1$^{st}$ Eigenvalue | 2$^{nd}$ Eigenvalue | 3$^{rd}$ Eigenvalue | 4$^{th}$ Eigenvalue |
| -0.23493 + 133.25i | -1.7942 + 823.8i | -6.8148 + 2176.6i | -16.545 + 3988.6i |
| Eigenvectors | | | |
| 1$^{st}$ Mode Shape | 2$^{nd}$ Mode Shape | 3$^{rd}$ Mode Shape | 4$^{th}$ Mode Shape |
| 0.6092 + 12.045i | -0.082 + 36.159i | 0.2498 + 38.618i | 0.3409 + 24.52i |
| 2.2789 + 43.483i | 0.35 + 58.868i | -0.1477 - 2.511i | -0.3567 - 25.192i |
| 4.3091 + 80.312i | 0.0654 + 8.9293i | -0.129 - 27.364i | 0.3148 + 23.475i |
| -1.7993 + 127.23i | 0.3726 - 82.348i | 0.2118 + 48.259i | -0.4452 - 34.297i |

**Table 4.9: Eigen-Properties for Undamaged Beam 8.**

| Eigenvalues | | | |
|---|---|---|---|
| 1$^{st}$ Eigenvalue | 2$^{nd}$ Eigenvalue | 3$^{rd}$ Eigenvalue | 4$^{th}$ Eigenvalue |
| -0.28276 + 134.97i | -1.7939 + 828.97i | -6.5754 + 2199.1i | -16.381 + 4017.8i |
| Eigenvectors | | | |
| 1$^{st}$ Mode Shape | 2$^{nd}$ Mode Shape | 3$^{rd}$ Mode Shape | 4$^{th}$ Mode Shape |
| -0.4759 + 15.516i | 0.0199 + 39.006i | 0.0625 + 39.702i | 0.2541 + 23.954i |
| 0.3833 + 45.362i | 0.0312 + 63.626i | -0.1407 - 1.42i | -0.3228 - 25.994i |
| -5.0334 + 87.647i | -0.0598 + 9.8517i | -0.0618 - 28.879i | 0.2451 + 23.267i |
| 5.181 + 133.93i | 0.5268 - 86.744i | 0.1372 + 49.523i | -0.339 - 33.109i |

**Table 4.10: Eigen-Properties for Damaged Beam 8.**

| Eigenvalues | | | |
|---|---|---|---|
| 1$^{st}$ Eigenvalue | 2$^{nd}$ Eigenvalue | 3$^{rd}$ Eigenvalue | 4$^{th}$ Eigenvalue |
| -0.24083 + 134.92i | -1.8106 + 826.36i | -6.6998 + 2203.2i | -16.514 + 4014.2i |
| Eigenvectors | | | |
| 1$^{st}$ Mode Shape | 2$^{nd}$ Mode Shape | 3$^{rd}$ Mode Shape | 4$^{th}$ Mode Shape |
| 0.4054 + 14.722i | 0 + 39.189i | 0.3864 + 37.343i | 0.7904 + 20.514i |
| -0.6759 + 39.963i | 0.517 + 54.706i | -0.1707 - 1.6522i | -0.8738 - 23.117i |
| 1.9663 + 76.159i | 0.0305 + 8.6751i | -0.4329 - 24.942i | 0.6267 + 22.21i |
| 4.3413 + 121.99i | -1.4653 - 79.775i | 0.7239 + 45.461i | -1.0951 - 28.918i |

Finite Element Model Reduction

Finite element techniques were used to construct a model that will properly described the cantilever beam system. Mass and stiffness matrices were assembled using the theory presented in Chapter Three. The beam was divided into 4 elements. Each element had two nodes, with two degrees of freedom in each node. Translational degrees

of freedom are designated as master degrees of freedom, while rotational degrees are designated as slave degrees of freedom. Each element is represented by a 4 by 4 mass matrix and a 4 by 4 stiffness matrix system. Using the superposition principle the global matrices are assembled, yielding 10 by 10 mass and stiffness matrices. Applying boundary conditions to the system, the matrices reduce to an eight degrees of freedom system.

Because only the translation degrees of freedom can be measured, the system is further reduced using the Iterated Improved Reduced System (*IIRS*) described in Chapter 3. This method was chosen because of its advantages over other methods such as the Guyan Reduction Method. The global matrices terms are rearranged according to equation 3.27. The resulting reduced matrices are presented next.

**Beam 5**

$$
M = \begin{bmatrix}
1.6578 & 0.2098 & -0.1162 & 0.07748 \\
0.2098 & 1.7789 & 0.1378 & -0.1279 \\
-0.1162 & 0.1378 & 1.8497 & 0.3051 \\
0.07748 & -0.1279 & 0.3051 & 0.5621
\end{bmatrix} 10^{-2}
\quad
K = \begin{bmatrix}
123020 & -77265 & 28671 & -4556.7 \\
-77265 & 93570 & -62341 & 16844 \\
28671 & -62341 & 64476 & -23788 \\
-4556.7 & 16844 & -23788 & 10485
\end{bmatrix}
$$

**Beam 6**

$$
M = \begin{bmatrix}
1.6511 & 0.2090 & -0.1157 & 0.07718 \\
0.2090 & 1.7718 & 0.1372 & -0.1274 \\
-0.1157 & 0.1372 & 1.8423 & 0.3039 \\
0.07718 & -0.1274 & 0.3039 & 0.5599
\end{bmatrix} 10^{-2}
\quad
K = \begin{bmatrix}
123010 & -77254 & 28667 & -4556.1 \\
-77254 & 93558 & -62333 & 16842 \\
28667 & -62333 & 64467 & -23785 \\
-4556.1 & 16842 & -23785 & 10483
\end{bmatrix}
$$

**Beam 8**

$$
M = \begin{bmatrix}
1.6282 & 0.2061 & -0.1141 & 0.0761 \\
0.2061 & 1.7472 & 0.1353 & -0.1256 \\
-0.1141 & 0.1353 & 1.8167 & 0.2997 \\
0.0761 & -0.1256 & 0.2997 & 0.5521
\end{bmatrix} 10^{-2}
\quad
K = \begin{bmatrix}
119690 & -75169 & 27893 & -4433.1 \\
-75169 & 91032 & -60650 & 16387 \\
27893 & -60650 & 62727 & -23143 \\
-4433.1 & 16387 & -23143 & 10200
\end{bmatrix}
$$

In addition to these reduced matrices, a second mass matrix will be used to generate another model. This mass matrix will be composed of only the terms corresponding to the master degrees of freedom. The purpose of this is to generate a model that will not be dependant upon a stiffness matrix in order to be reduced. In order to estimate this mass matrix, only the mass density of the beam is necessary. The *FRF's*

corresponding to this model, call lumped mass parameter model, will be compared with those of the other models to verify its validity.

This mass matrix is defined as:

$$M_{Lumped} = \frac{\overline{m} \cdot l}{420} \begin{bmatrix} 312 & 54 & 0 & 0 \\ 54 & 312 & 54 & 0 \\ 0 & 54 & 312 & 54 \\ 0 & 0 & 54 & 156 \end{bmatrix} \tag{4.6}$$

where $\overline{m}$ is the mass per unit length of the beam and $l$ is the length of the element.

This chapter presented the steps to follow in order to obtain the necessary preliminary data used to update the models for the beams. From this data the stiffness matrix can be updated and the damping matrix identified. The next step in the process would be to generate *FRF* plots for the beams in both damage scenarios, so that the model could be compared with the experimental data, therefore validating the process. The process is summarized in the following flowchart.
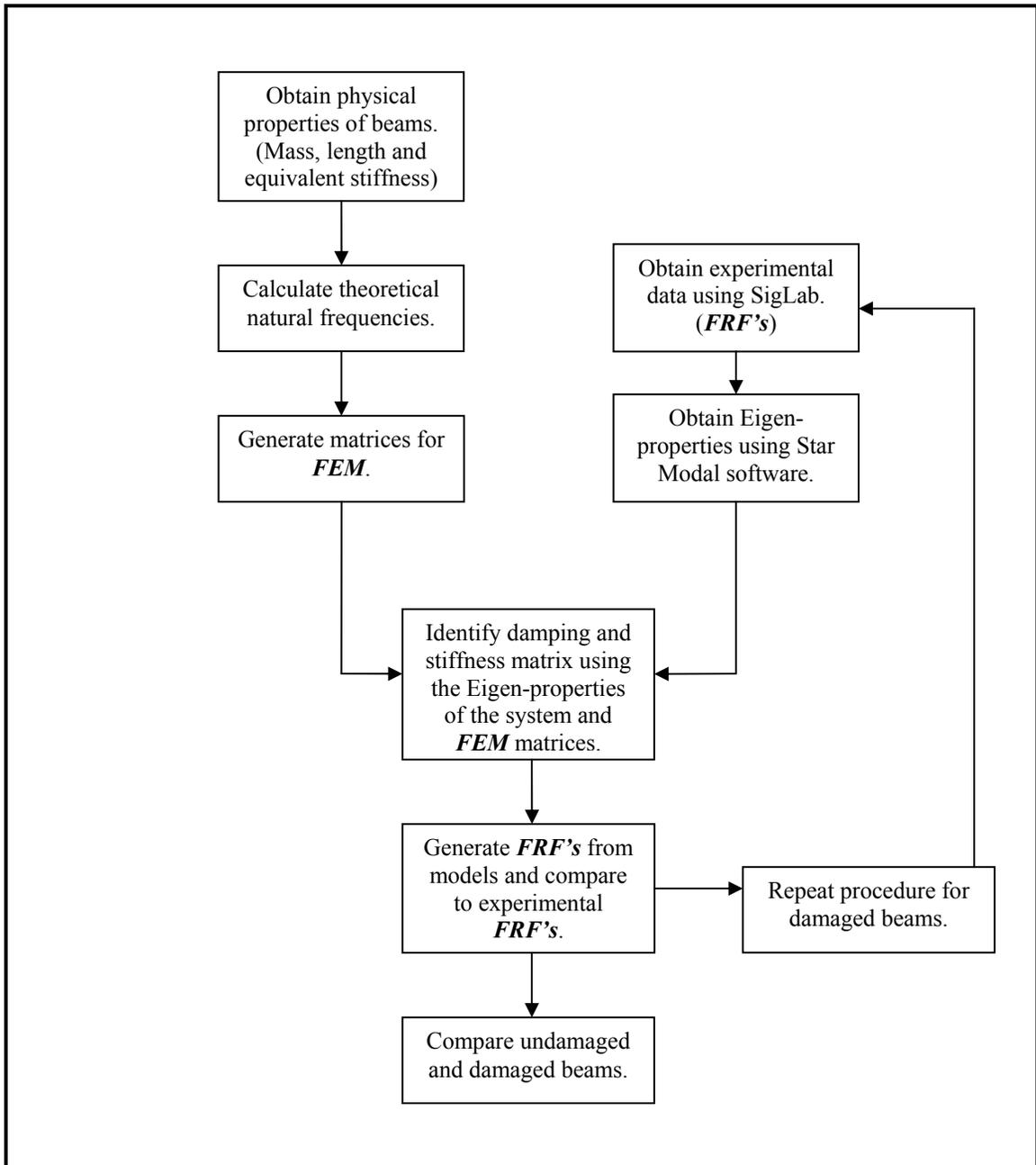
**Figure 4.6: Procedure Flowchart.**

**Chapter Five:**

**Examples**

Two examples are presented in this chapter is to demonstrate the damping and stiffness updating procedure. The first example is represented by a simple lumped mass model. The masses in the system are coupled using a spring and a damper. The iterative process of identifying and updating the damping and stiffness matrices are explained. Using the correctly identified damping matrix, the stiffness matrix for the system is also updated. The second example will be a model of a four element cantilever beam. This situation resembles closely the experimental situation in this investigation. The data is taken from Ortiz [3].

Example 1: Lumped Mass System

Consider the two degree of freedom system presented in Figure 5.1.
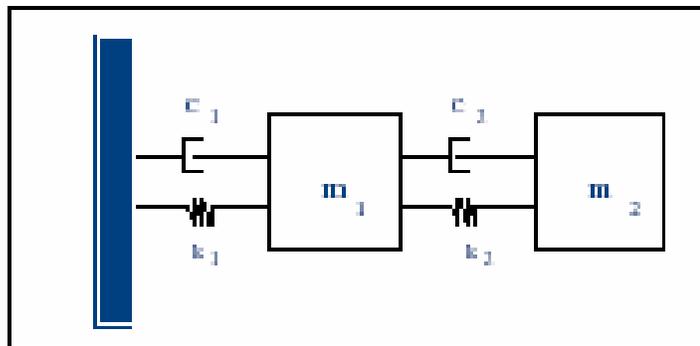


**Figure 5.1: Two Degree of Freedom Lumped Mass System.**

The parameters of the system are $m_1$, $m_2$, $c_1$, $c_2$, $k_1$ and $k_2$ which are the system's mass, damping and stiffness coefficients respectively. Application of Newton's second law of motion yields a linear matrix equation of the form:

$$[m]\{\ddot{x}\} + [c]\{\dot{x}\} + [k]\{x\} = 0 \tag{5.1}$$

The matrices $[m]$, $[c]$ and $[k]$ are the system's mass, damping and stiffness matrices and are given by:

$$M = \begin{bmatrix} 5 & 0 \\ 0 & 5 \end{bmatrix},$$

$$C = \begin{bmatrix} 0.02 & -0.01 \\ -0.01 & 0.01 \end{bmatrix}$$

and

$$K = \begin{bmatrix} 3 & -1.5 \\ -1.5 & 1.5 \end{bmatrix}.$$

Here the values of $m_1$, $m_2$, $c_1$, $c_2$, $k_1$ and $k_2$ have been arbitrarily assigned as 5 kg, 0.01 N·s/m and 1.5 N/m.

In this example, we will assume that the mass matrix is previously known and the damping and stiffness will be determined using the procedure described in the previous chapter. It is assumed that the eigen-properties are obtained experimentally. Because we know the system's properties, we know the values of the eigenvalues and eigenvectors of the system. These eigenvalues and eigenvectors occur in complex conjugates, so only one value from each pair is needed. The eigen-properties for this example are:

$$\Lambda = \begin{bmatrix} -0.00038197 + 0.33851i & 0 \\ 0 & -0.002618 + 0.88623i \end{bmatrix}$$

$$\Phi = \begin{bmatrix} 0.49797 + 1.2495e - 17i & -0.63662 \\ 0.80574 & 0.39345 - 1.8215e - 17i \end{bmatrix}$$

For the iterative process, the data that will be used is the mass matrix of the system, along with the eigenvalues and eigenvectors of the system. As an initial step, we choose a preliminary damping matrix. Here, the identity matrix was chosen as the initial matrix.

$$C_0 = \begin{bmatrix} 1 & 0 \\ 0 & 1 \end{bmatrix}$$

Next, the eigenvectors are normalized according to

$$\phi_i^T \left( 2M\lambda_i + C \right)\phi_i = 1 \tag{5.2}$$

After normalizing the eigenvectors, the new damping matrix is calculated using the following equation:

$$C = -M\left(\Phi\Lambda^2\Phi^T + \overline{\Phi\Lambda^2\Phi^T}\right)M \,. \tag{5.3}$$

Here the term $\overline{\Phi}$ is the conjugate of the eigenvector matrix and $\overline{\Lambda}$ is the conjugate of the eigenvalue matrix.

After the first iteration, the new damping matrix was given by:

$$C_1 = \begin{bmatrix} 0.4945 & -0.0202 \\ -0.0202 & 0.4744 \end{bmatrix}.$$

Using this new damping matrix, the eigenvectors are again normalized and the process is repeated. The following matrices are the damping matrices for iterations 5 and 10 respectively.

$$C_5 = \begin{bmatrix} 0.0494 & -0.0109 \\ -0.0109 & 0.0385 \end{bmatrix}$$

$$C_{10} = \begin{bmatrix} 0.0209 & -0.0100 \\ -0.0100 & 0.0109 \end{bmatrix}$$

At the sixteenth iteration convergence with the real value of the damping matrix is obtained which is given by:

$$C_{16} = \begin{bmatrix} 0.02 & -0.01 \\ -0.01 & 0.01 \end{bmatrix}.$$

With this iterated damping matrix and the normalized eigenvectors corresponding to this iteration, we can identify the stiffness matrix using the following equation.

$$K = \left(-\Phi\Lambda^{-1}\Phi^T - \overline{\Phi\Lambda^{-1}\Phi^T}\right)^{-1} \tag{5.4}$$

Using the eigenvectors normalized by the converged damping matrix, the resulting stiffness matrix is

$$K = \begin{bmatrix} 3.0 & -1.5 \\ -1.5 & 1.5 \end{bmatrix}.$$

This is equivalent to the original stiffness matrix of the system using Newton's second law.

Example 2: A Cantilever Composite Beam

To further illustrate the effectiveness of the damping and stiffness updating process, consider the following example. A composite beam is composed of a honeycomb and foam core faced with carbon fiber sheets. The beam is modeled using finite element techniques. The beam is divided into four elements with two nodes per element. Each node has 2 *DOF*, one translational *DOF* and one rotational *DOF*. The beam is cantilevered and the original mass and stiffness matrices were reduced using the *IIRS* scheme, yielding a four by four system. The data for this example comes from Ortiz (2002). Refer to Figure 5.2 for a beam schematic.
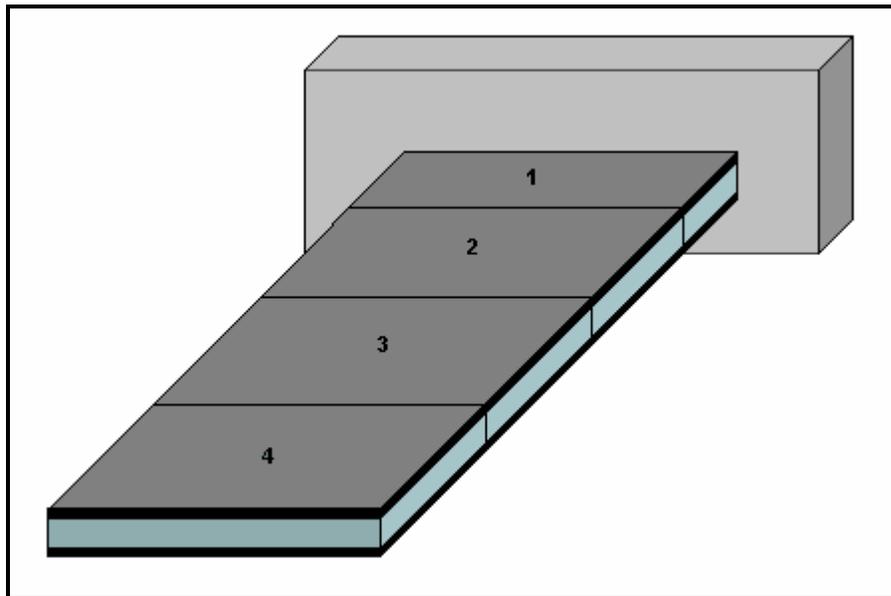


**Figure 5.2: Composite Cantilever Beam.**

The reduced mass and stiffness matrices are:

$$M = \begin{bmatrix} 0.0123 & 0.0015 & -0.0008 & 0.0005 \\ 0.0015 & 0.0132 & 0.0010 & -0.0009 \\ -0.0008 & 0.0010 & 0.0137 & 0.0022 \\ 0.0005 & -0.0009 & 0.0022 & 0.0040 \end{bmatrix}$$

$$K = \begin{bmatrix} 5.6864 & -3.5687 & 1.3255 & -0.2117 \\ -3.5687 & 4.3251 & -2.8827 & 0.7791 \\ 1.3255 & -2.8827 & 2.9829 & -1.1009 \\ -0.2117 & 0.7791 & -1.1009 & 0.4854 \end{bmatrix} \cdot 10^4$$

The damping matrix was successfully identified by Ortiz as:

$$C = \begin{bmatrix} -0.2509 & -0.1670 & 0.1051 & 0.0330 \\ -0.1670 & 0.0767 & 0.2053 & 0.0704 \\ 0.1051 & 0.2053 & -0.0582 & 0.0480 \\ 0.0330 & 0.0704 & 0.0480 & 0.0346 \end{bmatrix} \quad\quad (5.5)$$

From testing of the beam the following eigen-properties were obtained.

$$\lambda_1 = -7.9026 + 99.286i, \quad \phi_1 = \begin{bmatrix} -6.81 \cdot 10^{-5} - 7.81 \cdot 10^{-4} i \\ -2.29 \cdot 10^{-4} - 2.72 \cdot 10^{-3} i \\ -4.26 \cdot 10^{-4} - 5.28 \cdot 10^{-3} i \\ -6.38 \cdot 10^{-4} - 8.02 \cdot 10^{-3} i \end{bmatrix}$$

$$\lambda_2 = 5.6623 + 625.66i, \quad \phi_2 = \begin{bmatrix} 1.53 \cdot 10^{-5} - 5.08 \cdot 10^{-4} i \\ 2.18 \cdot 10^{-5} - 8.65 \cdot 10^{-4} i \\ 8.08 \cdot 10^{-6} - 1.52 \cdot 10^{-4} i \\ -1.12 \cdot 10^{-5} + 1.23 \cdot 10^{-3} i \end{bmatrix}$$

$$\lambda_3 = 7.692 + 1764.3i, \quad \phi_3 = \begin{bmatrix} -4.2 \cdot 10^{-6} - 2.98 \cdot 10^{-4} i \\ -2.4 \cdot 10^{-6} - 6.51 \cdot 10^{-4} i \\ 1.99 \cdot 10^{-6} + 2.36 \cdot 10^{-4} i \\ 1.83 \cdot 10^{-6} - 4.20 \cdot 10^{-4} i \end{bmatrix}$$

$$\lambda_4 = -0.0038 + 3422.6i, \quad \phi_4 = \begin{bmatrix} 1.33 \cdot 10^{-7} + 1.31 \cdot 10^{-4} i \\ 3.36 \cdot 10^{-7} - 1.97 \cdot 10^{-4} i \\ 7.10 \cdot 10^{-7} + 1.18 \cdot 10^{-4} i \\ -2.11 \cdot 10^{-10} - 1.88 \cdot 10^{-4} i \end{bmatrix}$$

The input data needed to update the damping and stiffness matrices are the mass matrix of the system and the eigen-properties of the system. Following the same procedure as in Example 1, the initial damping matrix is chosen as the identity matrix.

$$C_0 = \begin{bmatrix} 1 & 0 & 0 & 0 \\ 0 & 1 & 0 & 0 \\ 0 & 0 & 1 & 0 \\ 0 & 0 & 0 & 1 \end{bmatrix}$$

By normalizing the eigenvectors of the system, as in equation 5.2, and substituting into equation 5.3, the first iterated damping matrix is obtained. This result will be used to again normalize the eigenvectors in order to find a new damping matrix. The following matrices correspond to iterations: 1, 5, 10, 15 and 20 and are given by:

$$C_1 = \begin{bmatrix} 0.6696 & -0.1447 & 0.0082 & 0.0580 \\ -0.1447 & 0.9548 & 0.1203 & -0.0214 \\ 0.0082 & 0.1203 & 0.6188 & 0.0412 \\ 0.0580 & -0.0214 & 0.0412 & 0.2489 \end{bmatrix},$$

$$C_5 = \begin{bmatrix} -0.1937 & -0.1660 & 0.0988 & 0.0345 \\ -0.1660 & 0.1306 & 0.1992 & 0.0645 \\ 0.0988 & 0.1992 & -0.0182 & 0.0466 \\ 0.0345 & 0.0645 & 0.0466 & 0.0474 \end{bmatrix},$$

$$C_{10} = \begin{bmatrix} -0.2494 & -0.1673 & 0.1049 & 0.0331 \\ -0.1673 & 0.0777 & 0.2051 & 0.0749 \\ 0.1049 & 0.2051 & -0.0571 & 0.0479 \\ 0.0331 & 0.0704 & 0.0479 & 0.0349 \end{bmatrix},$$

$$C_{15} = \begin{bmatrix} -0.2511 & -0.1673 & 0.1051 & 0.0331 \\ -0.1673 & 0.0761 & 0.2053 & 0.0706 \\ 0.1051 & 0.2053 & -0.0583 & 0.0480 \\ 0.0331 & 0.0706 & 0.0480 & 0.0345 \end{bmatrix}$$

and

$$C_{20} = \begin{bmatrix} -0.2512 & -0.1673 & 0.1051 & 0.0331 \\ -0.1673 & 0.0760 & 0.2053 & 0.0706 \\ 0.1051 & 0.2053 & -0.0583 & 0.0480 \\ 0.0331 & 0.0706 & 0.0480 & 0.0345 \end{bmatrix}$$

respectively.

After 20 iterations, the damping matrix converged to what Ortiz obtained, given by equation 5.5. The stiffness matrix identified by the algorithm after the twentieth iteration is

$$K = \begin{bmatrix} 5.6863 & -3.5687 & 1.3256 & -0.2118 \\ -3.5687 & 4.3252 & -2.8827 & 0.7791 \\ 1.3256 & -2.8827 & 2.9829 & -1.1009 \\ -0.2118 & 0.7791 & -1.1009 & 0.4854 \end{bmatrix} \cdot 10^4,$$

which is exact as Ortiz's results to the $3^{rd}$ decimal place and within the significant digits of accuracy of most equipment used in vibration modeling.

**Chapter Six:**

**Results and Discussion**

In this chapter the resulting model for the beams along with their *FRF* plots are presented. Each plot will show the experimental *FRF* along with the *FRF* plots corresponding to the different models: one model uses a reduced mass matrix with its resultant damping and stiffness matrices; the other model uses a lumped mass matrix and its corresponding damping and stiffness matrices. These graphs show the adequacy of the method in identifying the damping and stiffness matrices creating a model capable of describing accurately the dynamic behavior of the cantilever composite beams that were investigated.

The following pages present the results for each of the beams. The final models for the beams will be shown along with their corresponding *FRF* plots. This will be done for both the undamaged and the damaged scenarios. Finally a graph with the experimental plots corresponding to the undamaged and damaged condition will be shown.

Beam 5

Undamaged Beam:

Reduced mass model

$$[M] = \begin{bmatrix} 0.016578 & 0.002098 & -0.001162 & 0.000775 \\ 0.002098 & 0.01779 & 0.001378 & -0.001279 \\ -0.001162 & 0.001378 & 0.01850 & 0.003051 \\ 0.000775 & -0.001279 & 0.003051 & 0.005621 \end{bmatrix} [C] = \begin{bmatrix} 0.1979 & -0.1055 & -0.1152 & -0.1032 \\ -0.1055 & 0.0591 & -0.1429 & 0.0101 \\ -0.1152 & -0.1429 & 0.3399 & -0.0510 \\ -0.1032 & 0.0101 & -0.0510 & 0.0227 \end{bmatrix}$$

$$[K] = \begin{bmatrix} 1.0250 & -0.6194 & 0.2252 & -0.0298 \\ -0.6194 & 0.8195 & -0.5902 & 0.1536 \\ 0.2252 & -0.5902 & 0.6778 & -0.2464 \\ -0.0298 & 0.1536 & -0.2464 & 0.1080 \end{bmatrix} \cdot 10^5$$

Lumped mass model

$$[M] = \begin{bmatrix} 0.015 & 2.537 \cdot 10^{-3} & 0 & 0 \\ 2.537 \cdot 10^{-3} & 0.015 & 2.537 \cdot 10^{-3} & 0 \\ 0 & 2.537 \cdot 10^{-3} & 0.015 & 2.537 \cdot 10^{-3} \\ 0 & 0 & 2.537 \cdot 10^{-3} & 7.33 \cdot 10^{-3} \end{bmatrix} [C] = \begin{bmatrix} 0.2378 & -0.1041 & -0.1119 & -0.1307 \\ -0.1041 & 0.0048 & -0.0830 & 0.0268 \\ -0.1119 & -0.0830 & 0.2123 & -0.1016 \\ -0.1307 & 0.0268 & -0.1016 & 0.0987 \end{bmatrix}$$

$$[K] = \begin{bmatrix} 9.9430 & -6.4000 & 2.7396 & -0.5060 \\ -6.4000 & 8.3999 & -6.0891 & 1.6050 \\ 2.7396 & -6.0891 & 6.7054 & -2.3997 \\ -0.5060 & 1.6050 & -2.3997 & 1.0362 \end{bmatrix} \cdot 10^{4}$$
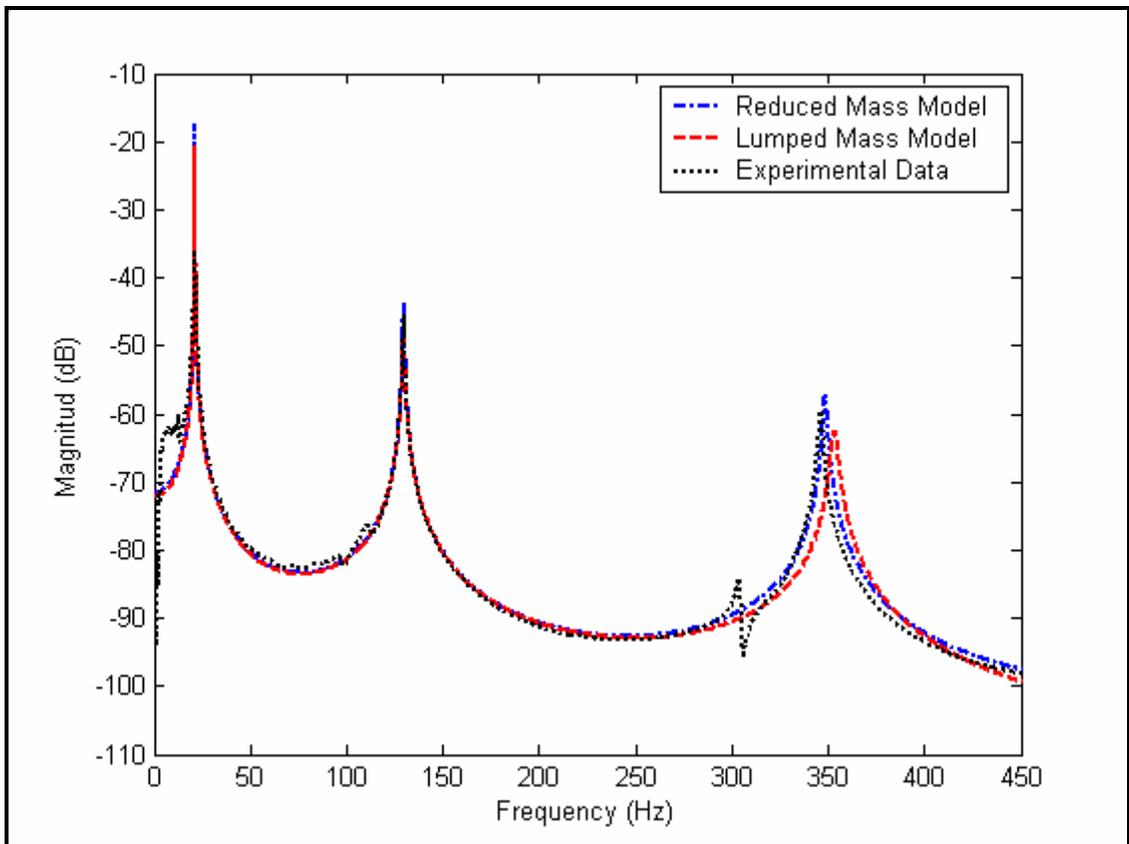


**Figure 6.1: Beam 5 Undamaged Condition – FEM Models vs. Experimental Data.**

**Table 6.1: Results for Undamaged Beam 5.**

| Natural Frequencies (Hz) | Experimental Data | Reduced Mass Model | Error (%) | Lumped Mass Model | Error (%) |
|---|---|---|---|---|---|
| 1st Natural Frequency | 21.536 | 21.392 | 0.67 | 21.523 | 0.06 |
| 2nd Natural Frequency | 129.721 | 129.869 | 0.11 | 129.834 | 0.09 |
| 3rd Natural Frequency | 346.148 | 348.614 | 0.71 | 353.519 | 2.13 |

Damaged Beam: damage was induced using a milling machine at ¼ the length of the beam from the fixed end.

Reduced mass model

$$[M] = \begin{bmatrix} 0.016578 & 0.002098 & -0.001162 & 0.000775 \\ 0.002098 & 0.01779 & 0.001378 & -0.001279 \\ -0.001162 & 0.001378 & 0.01850 & 0.003051 \\ 0.000775 & -0.001279 & 0.003051 & 0.005621 \end{bmatrix} \quad [C] = \begin{bmatrix} 0.2905 & 0.0294 & -0.0024 & -0.0091 \\ 0.0294 & 0.1681 & -0.2151 & 0.0635 \\ -0.0024 & -0.2151 & 0.1279 & -0.0385 \\ -0.0091 & 0.0635 & -0.0385 & 0.0329 \end{bmatrix}$$

$$[K] = \begin{bmatrix} 1.0036 & -0.6037 & 0.2103 & -0.0281 \\ -0.6037 & 0.8307 & -0.6018 & 0.1704 \\ 0.2103 & -0.6018 & 0.6837 & -0.2641 \\ -0.0281 & 0.1704 & -0.2641 & 0.1215 \end{bmatrix} \cdot 10^5$$

Lumped mass model

$$[M] = \begin{bmatrix} 0.015 & 2.537 \cdot 10^{-3} & 0 & 0 \\ 2.537 \cdot 10^{-3} & 0.015 & 2.537 \cdot 10^{-3} & 0 \\ 0 & 2.537 \cdot 10^{-3} & 0.015 & 2.537 \cdot 10^{-3} \\ 0 & 0 & 2.537 \cdot 10^{-3} & 7.33 \cdot 10^{-3} \end{bmatrix} \quad [C] = \begin{bmatrix} 0.2793 & 0.0206 & 0.0089 & -0.0325 \\ 0.0206 & 0.1215 & -0.1271 & 0.1196 \\ 0.0089 & -0.1271 & 0.0746 & -0.0576 \\ -0.0325 & 0.1196 & -0.0576 & 0.1188 \end{bmatrix}$$

$$[K] = \begin{bmatrix} 9.7321 & -6.2793 & 2.6228 & -0.5135 \\ -6.2793 & 8.5406 & -6.2126 & 1.7790 \\ 2.6228 & -6.2126 & 6.7508 & -2.5679 \\ -0.5135 & 1.7790 & -2.5679 & 1.1633 \end{bmatrix} \cdot 10^4$$
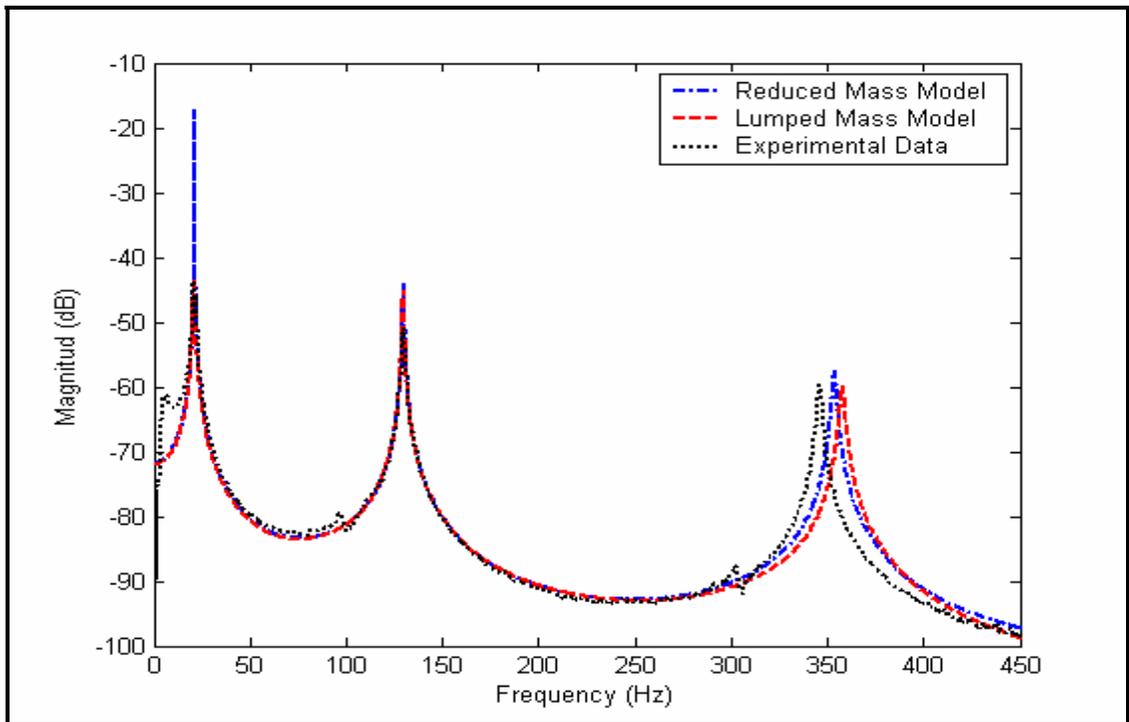
**Figure 6.2: Beam 5 Damaged Condition – FEM Models vs. Experimental Data.**
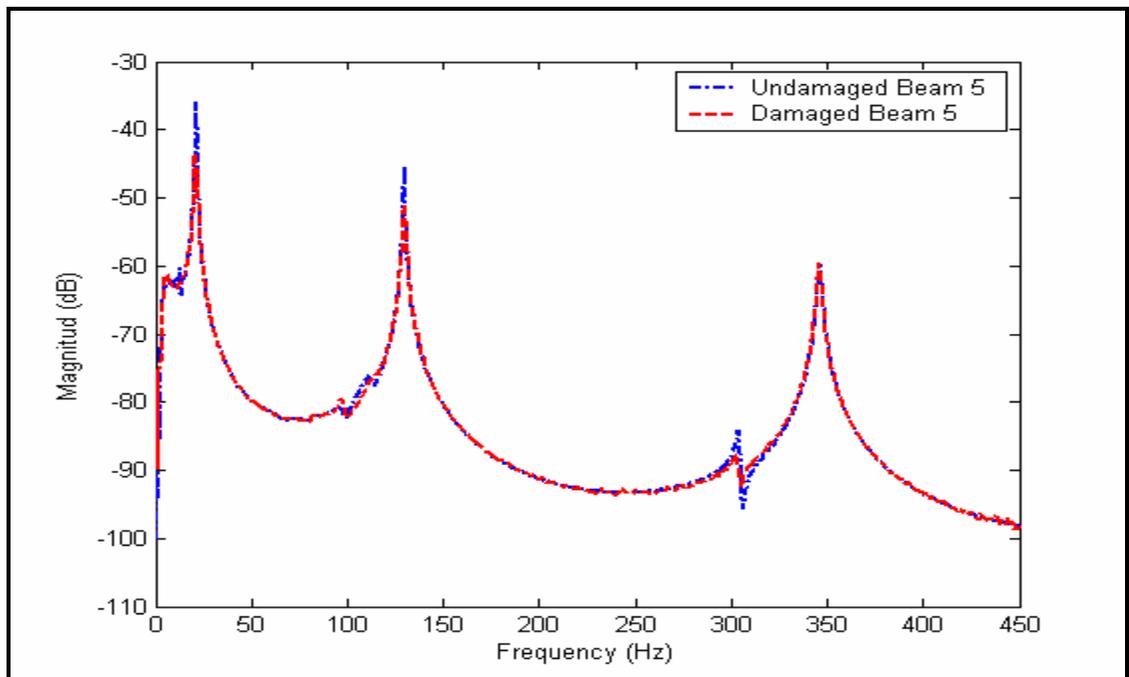


**Figure 6.3: Beam 5 - Experimental Data for Undamaged and Damaged Conditions.**

**Table 6.2: Results for Damaged Beam 5.**

| Natural Frequencies (Hz) | Experimental Data | Reduced Mass Model | Error (%) | Lumped Mass Model | Error (%) |
|---|---|---|---|---|---|
| 1st Natural Frequency | 21.193 | 21.279 | 0.41 | 21.188 | 0.02 |
| 2nd Natural Frequency | 129.807 | 129.946 | 0.11 | 129.771 | 0.03 |
| 3rd Natural Frequency | 345.922 | 353.803 | 2.28 | 357.926 | 3.47 |

<u>Beam 6</u>

Undamaged Beam:

Reduced mass model

$$[M] = \begin{bmatrix} 0.016511 & 0.002089 & -0.001157 & 0.000772 \\ 0.002089 & 0.01772 & 0.001372 & -0.001273 \\ -0.001157 & 0.001372 & 0.01842 & 0.003039 \\ 0.000772 & -0.001273 & 0.003039 & 0.005599 \end{bmatrix} [C] = \begin{bmatrix} 0.2097 & -0.0754 & -0.0157 & 0.0016 \\ -0.0754 & 0.2497 & -0.1302 & 0.0519 \\ -0.0157 & -0.1302 & 0.0736 & -0.0578 \\ 0.0016 & 0.0519 & -0.0578 & 0.0405 \end{bmatrix}$$

$$[K] = \begin{bmatrix} 9.9970 & -6.2135 & 1.9353 & -0.2679 \\ -6.2135 & 8.2353 & -5.3995 & 1.5545 \\ 1.9353 & -5.3995 & 5.9475 & -2.4122 \\ -0.2679 & 1.5545 & -2.4122 & 1.1686 \end{bmatrix} \cdot 10^4$$

Lumped mass model

$$[M] = \begin{bmatrix} 0.015 & 2.527 \cdot 10^{-3} & 0 & 0 \\ 2.527 \cdot 10^{-3} & 0.015 & 2.527 \cdot 10^{-3} & 0 \\ 0 & 2.527 \cdot 10^{-3} & 0.015 & 2.527 \cdot 10^{-3} \\ 0 & 0 & 2.527 \cdot 10^{-3} & 7.301 \cdot 10^{-3} \end{bmatrix} [C] = \begin{bmatrix} 0.1793 & -0.0282 & -0.0020 & -0.0239 \\ -0.0282 & 0.1951 & -0.0489 & 0.1056 \\ -0.0020 & -0.0489 & 0.0713 & -0.0395 \\ -0.0239 & 0.1056 & -0.0395 & 0.1440 \end{bmatrix}$$

$$[K] = \begin{bmatrix} 9.8598 & -6.5710 & 2.5038 & -0.5190 \\ -6.5710 & 8.6699 & -5.7711 & 1.6964 \\ 2.5038 & -5.7711 & 6.0484 & -2.4114 \\ -0.5190 & 1.6964 & -2.4114 & 1.1454 \end{bmatrix} \cdot 10^4$$
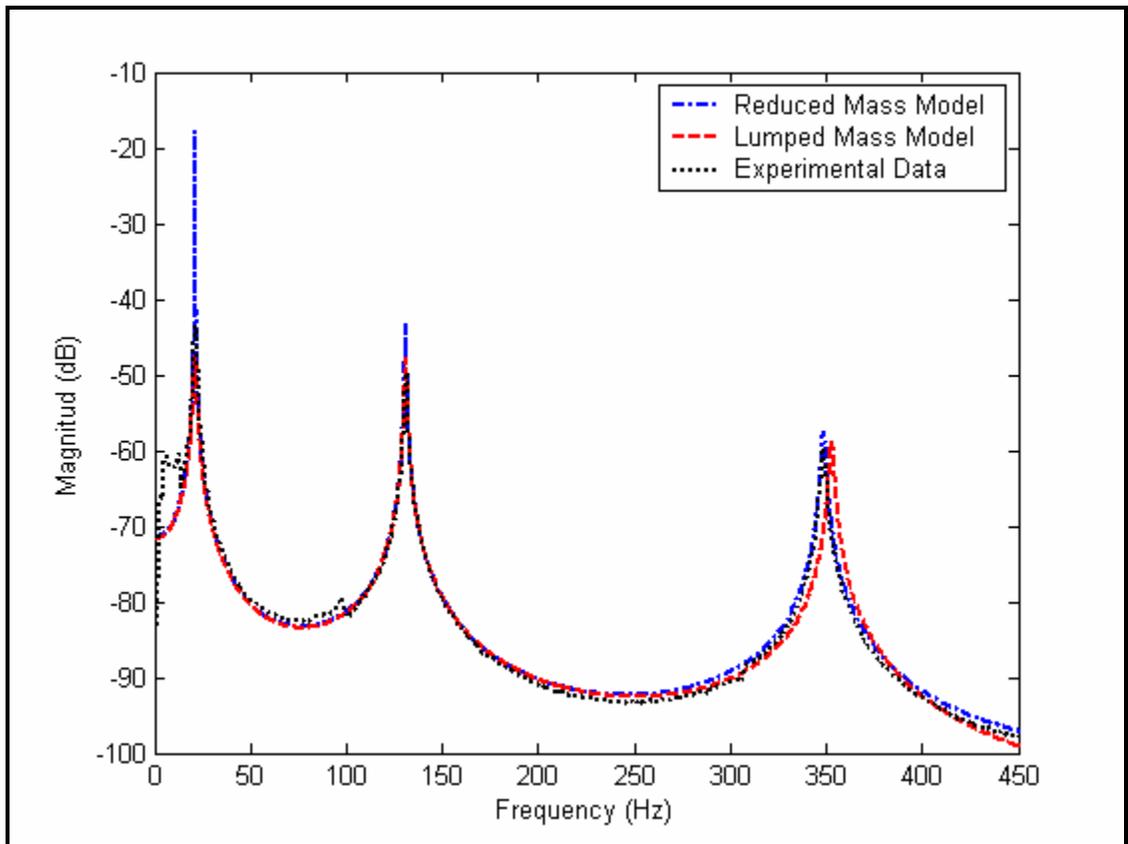
**Figure 6.4: Beam 6 Undamaged Condition – FEM Models vs. Experimental Data.**

**Table 6.3: Results for Undamaged Beam 6.**

| Natural Frequencies (Hz) | Experimental Data | Reduced Mass Model | Error (%) | Lumped Mass Model | Error (%) |
|---|---|---|---|---|---|
| 1st Natural Frequency | 21.4032 | 21.398 | 0.02 | 21.401 | 0.01 |
| 2nd Natural Frequency | 131.074 | 131.079 | 0.004 | 131.161 | 0.07 |
| 3rd Natural Frequency | 348.208 | 348.790 | 0.17 | 353.055 | 1.39 |

Damaged Beam: damage was induced using a milling machine at ¼ the length of the beam from the fixed end.

Reduced mass model

$$[M] = \begin{bmatrix} 0.016511 & 0.002089 & -0.001157 & 0.000772 \\ 0.002089 & 0.01772 & 0.001372 & -0.001273 \\ -0.001157 & 0.001372 & 0.01842 & 0.003039 \\ 0.000772 & -0.001273 & 0.003039 & 0.005599 \end{bmatrix} \quad [C] = \begin{bmatrix} 0.2695 & -0.0467 & 0.0130 & -0.0078 \\ -0.0467 & 0.0709 & -0.1946 & 0.0268 \\ 0.0130 & -0.1946 & 0.1243 & -0.0354 \\ -0.0078 & 0.0268 & -0.0354 & 0.0673 \end{bmatrix}$$

$$[K] = \begin{bmatrix} 9.6295 & -5.7762 & 2.0456 & -0.2254 \\ -5.7762 & 8.1187 & -6.1398 & 1.6621 \\ 2.0456 & -6.1398 & 7.4913 & -2.8028 \\ -0.2254 & 1.6621 & -2.8028 & 1.2373 \end{bmatrix} \cdot 10^4$$

Lumped mass model

$$[M] = \begin{bmatrix} 0.015 & 2.527 \cdot 10^{-3} & 0 & 0 \\ 2.527 \cdot 10^{-3} & 0.015 & 2.527 \cdot 10^{-3} & 0 \\ 0 & 2.527 \cdot 10^{-3} & 0.015 & 2.527 \cdot 10^{-3} \\ 0 & 0 & 2.527 \cdot 10^{-3} & 7.301 \cdot 10^{-3} \end{bmatrix} \quad [C] = \begin{bmatrix} 0.2541 & -0.0331 & 0.0249 & -0.0598 \\ -0.0331 & 0.0567 & -0.1255 & 0.0718 \\ 0.0249 & -0.1255 & 0.0736 & -0.0614 \\ -0.0598 & 0.0718 & -0.0614 & 0.1779 \end{bmatrix}$$

$$[K] = \begin{bmatrix} 9.4325 & -6.1135 & 2.6673 & -0.4846 \\ -6.1135 & 8.4911 & -6.4596 & 1.7706 \\ 2.6673 & -6.4596 & 7.4828 & -2.7478 \\ -0.4846 & 1.7706 & -2.7478 & 1.1914 \end{bmatrix} \cdot 10^4$$
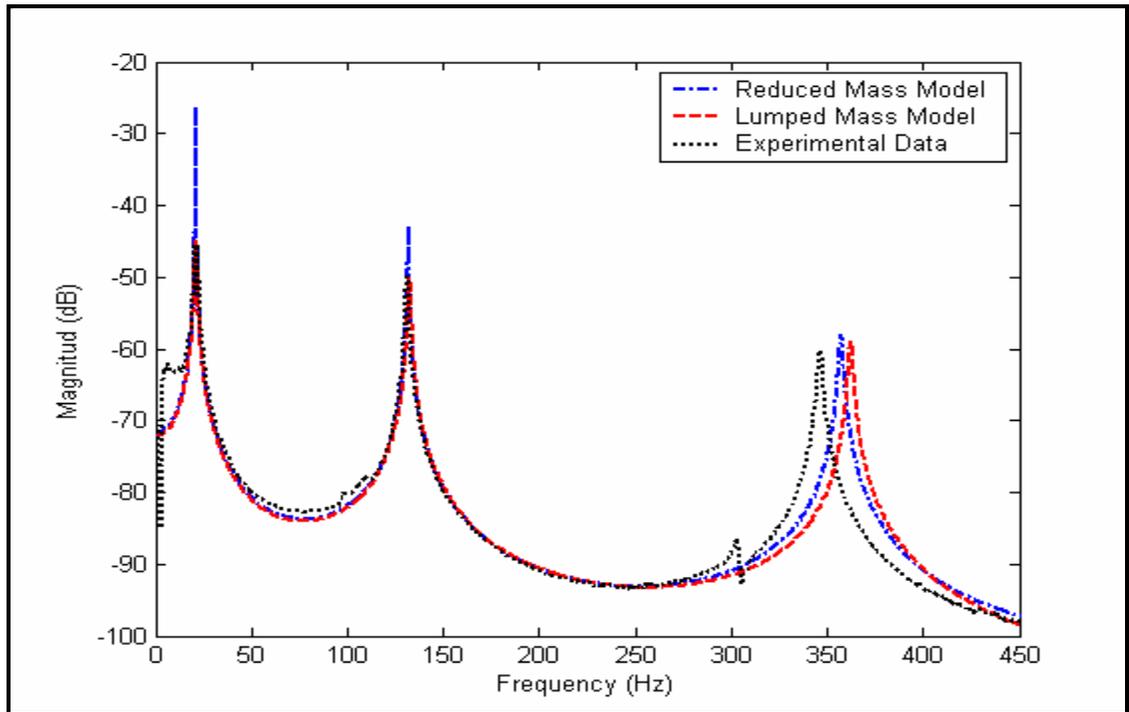
**Figure 6.5: Beam 6 Damaged Condition – FEM Models vs. Experimental Data.**
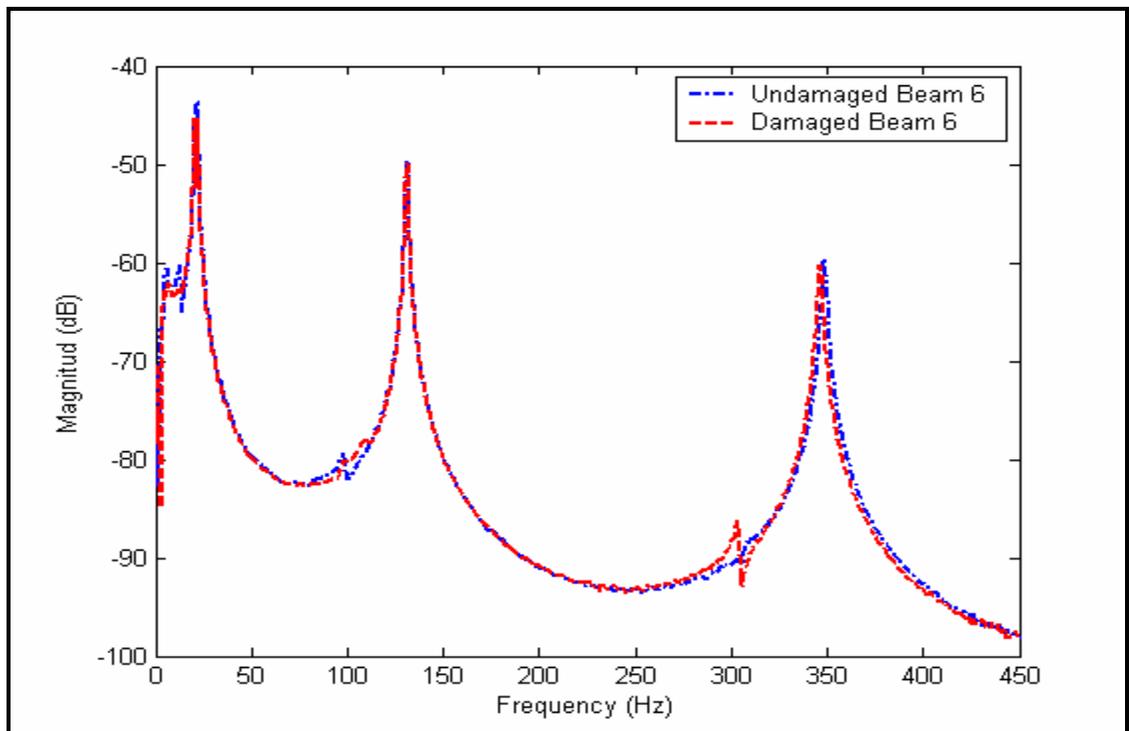


**Figure 6.6: Beam 6 - Experimental Data for Undamaged and Damaged Conditions.**

**Table 6.4: Results for Damaged Beam 6.**

| Natural Frequencies (Hz) | Experimental Data | Reduced Mass Model | Error (%) | Lumped Mass Model | Error (%) |
|---|---|---|---|---|---|
| 1st Natural Frequency | 21.208 | 21.184 | 0.11 | 21.224 | 0.08 |
| 2nd Natural Frequency | 131.112 | 132.08 | 0.74 | 132.527 | 1.08 |
| 3rd Natural Frequency | 346.412 | 357.336 | 3.15 | 362.429 | 4.62 |

Beam 8

Undamaged Beam:

Reduced mass model

$$[M] = \begin{bmatrix} 0.016282 & 0.002061 & -0.001141 & 0.000761 \\ 0.002061 & 0.01747 & 0.001353 & -0.001256 \\ -0.001141 & 0.001353 & 0.01817 & 0.002997 \\ 0.000761 & -0.001256 & 0.002997 & 0.005521 \end{bmatrix} [C] = \begin{bmatrix} 0.2899 & -0.0466 & 0.0384 & -0.0166 \\ -0.0466 & 0.0915 & -0.1388 & 0.0204 \\ 0.0384 & -0.1388 & 0.2387 & -0.0478 \\ -0.0166 & 0.0204 & -0.0478 & 0.0134 \end{bmatrix}$$

$$[K] = \begin{bmatrix} 1.1030 & -0.8503 & 0.4623 & -0.1424 \\ -0.8503 & 1.3537 & -1.1650 & 0.4047 \\ 0.4623 & -1.1650 & 1.3298 & -0.5277 \\ -0.1424 & 0.4047 & -0.5277 & 0.2266 \end{bmatrix} \cdot 10^5$$

Lumped mass model

$$[M] = \begin{bmatrix} 0.014 & 2.492 \cdot 10^{-3} & 0 & 0 \\ 2.492 \cdot 10^{-3} & 0.014 & 2.492 \cdot 10^{-3} & 0 \\ 0 & 2.492 \cdot 10^{-3} & 0.014 & 2.492 \cdot 10^{-3} \\ 0 & 0 & 2.492 \cdot 10^{-3} & 7.200 \cdot 10^{-3} \end{bmatrix} [C] = \begin{bmatrix} 0.2495 & -0.0082 & 0.0476 & -0.0560 \\ -0.0082 & 0.0645 & -0.0566 & 0.0493 \\ 0.0476 & -0.0566 & 0.1527 & -0.0596 \\ -0.0560 & 0.0493 & -0.0596 & 0.0864 \end{bmatrix}$$

$$[K] = \begin{bmatrix} 1.0399 & -0.8343 & 0.4830 & -0.1531 \\ -0.8343 & 1.2700 & -1.0648 & 0.3636 \\ 0.4830 & -1.0648 & 1.1702 & -0.4574 \\ -0.1531 & 0.3636 & -0.4574 & 0.1949 \end{bmatrix} \cdot 10^5$$
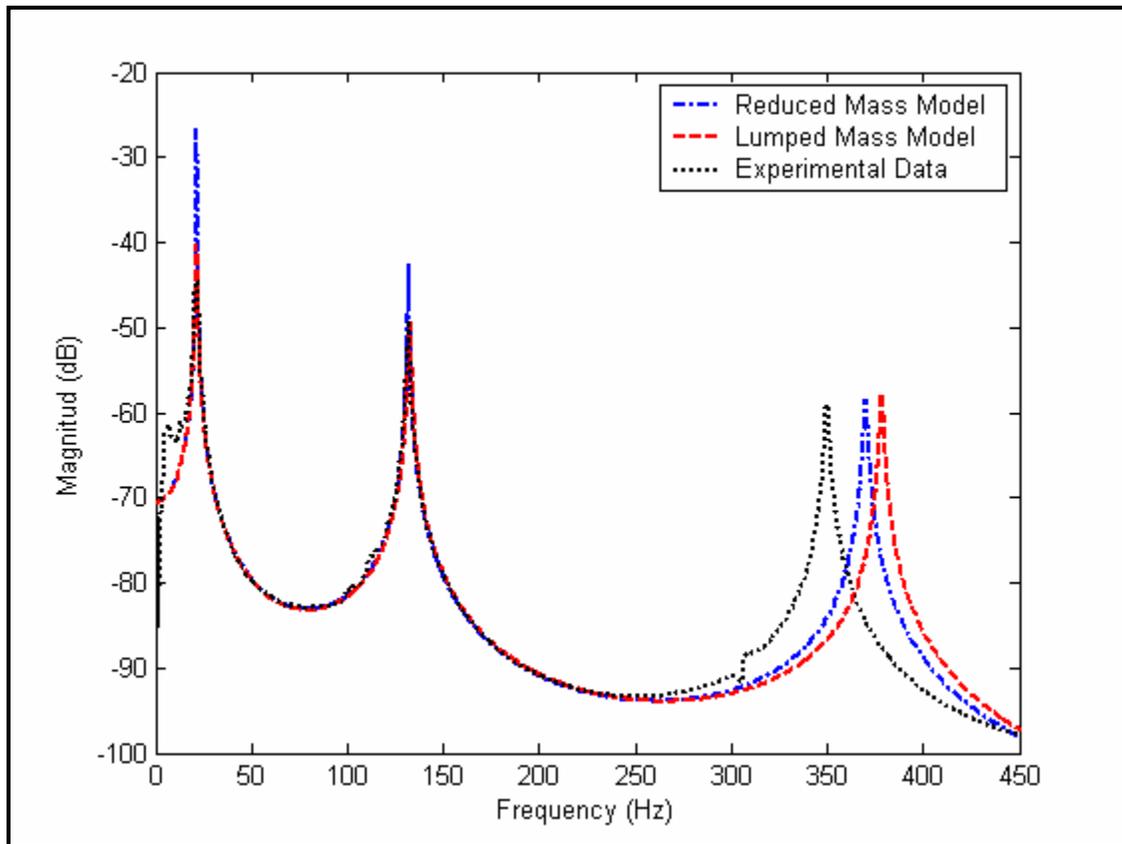
**Figure 6.7: Beam 8 Undamaged Condition – FEM Models vs. Experimental Data.**

**Table 6.5: Results for Undamaged Beam 8.**

| Natural Frequencies (Hz) | Experimental Data | Reduced Mass Model | Error (%) | Lumped Mass Model | Error (%) |
|---|---|---|---|---|---|
| 1st Natural Frequency | 21.481 | 21.696 | 1.00 | 21.600 | 0.55 |
| 2nd Natural Frequency | 131.935 | 132.14 | 0.16 | 132.77 | 0.63 |
| 3rd Natural Frequency | 350.004 | 370.228 | 5.78 | 378.663 | 8.19 |

Damaged Beam: damage was induced using a milling machine at ½ the length of the beam from the fixed end.

Reduced mass model

$$[M] = \begin{bmatrix} 0.016282 & 0.002061 & -0.001141 & 0.000761 \\ 0.002061 & 0.01747 & 0.001353 & -0.001256 \\ -0.001141 & 0.001353 & 0.01817 & 0.002997 \\ 0.000761 & -0.001256 & 0.002997 & 0.005521 \end{bmatrix} [C] = \begin{bmatrix} 0.3241 & 0.1888 & 0.1719 & 0.0654 \\ -0.0467 & 0.0916 & -0.2664 & 0.0261 \\ 0.0130 & -0.1946 & 0.4967 & -0.0020 \\ -0.0078 & 0.0268 & -0.0354 & -0.0218 \end{bmatrix}$$

$$[K] = \begin{bmatrix} 9.3892 & -6.4531 & 1.7496 & -0.1134 \\ -6.4531 & 9.1205 & -5.7623 & 1.4067 \\ 1.7496 & -5.7623 & 6.5157 & -2.3680 \\ -0.1134 & 1.4067 & -2.3680 & 1.0444 \end{bmatrix} \cdot 10^4$$

Lumped mass model

$$[M] = \begin{bmatrix} 0.014 & 2.492 \cdot 10^{-3} & 0 & 0 \\ 2.492 \cdot 10^{-3} & 0.014 & 2.492 \cdot 10^{-3} & 0 \\ 0 & 2.492 \cdot 10^{-3} & 0.014 & 2.492 \cdot 10^{-3} \\ 0 & 0 & 2.492 \cdot 10^{-3} & 7.200 \cdot 10^{-3} \end{bmatrix} [C] = \begin{bmatrix} 0.3209 & 0.1361 & 0.1678 & 0.0502 \\ 0.1361 & 0.0617 & -0.1740 & 0.0370 \\ 0.1678 & -0.1740 & 0.2332 & -0.1279 \\ 0.0502 & 0.0370 & -0.1279 & -0.0521 \end{bmatrix}$$

$$[K] = \begin{bmatrix} 8.5393 & -6.1015 & 1.9564 & -0.2504 \\ -6.1015 & 8.7095 & -5.5619 & 1.3681 \\ 1.9564 & -5.5619 & 6.0721 & -2.1782 \\ -0.2504 & 1.3681 & -2.1782 & 0.9548 \end{bmatrix} \cdot 10^4$$
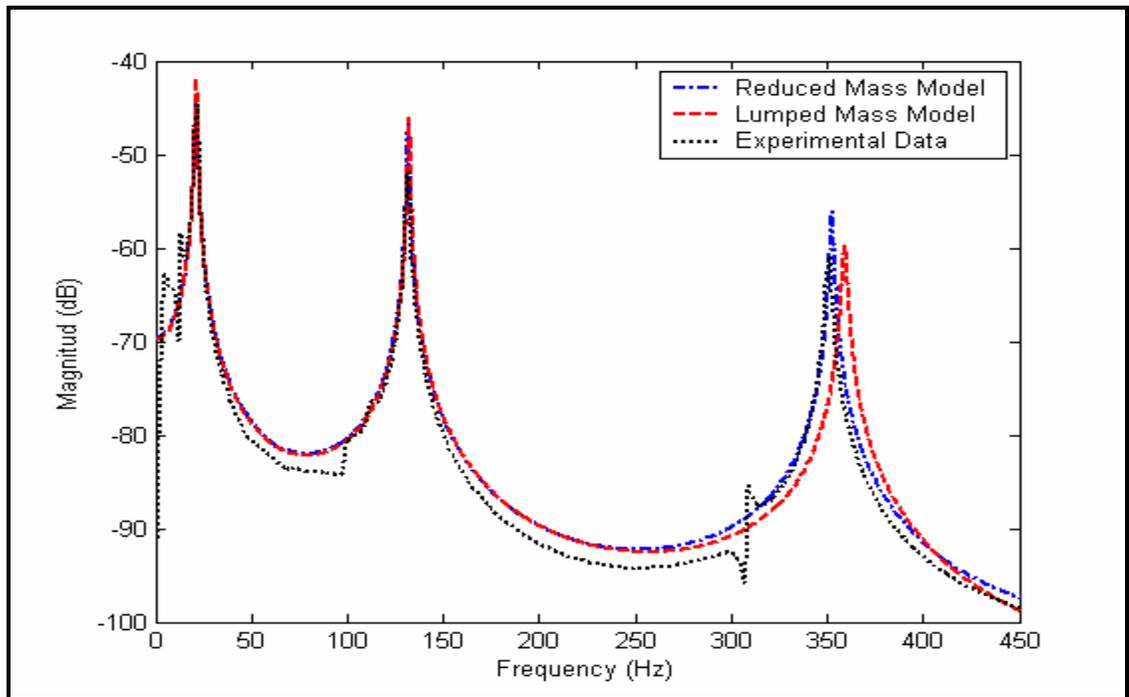
**Figure 6.8: Beam 8 Damaged Condition – FEM Models vs. Experimental Data.**
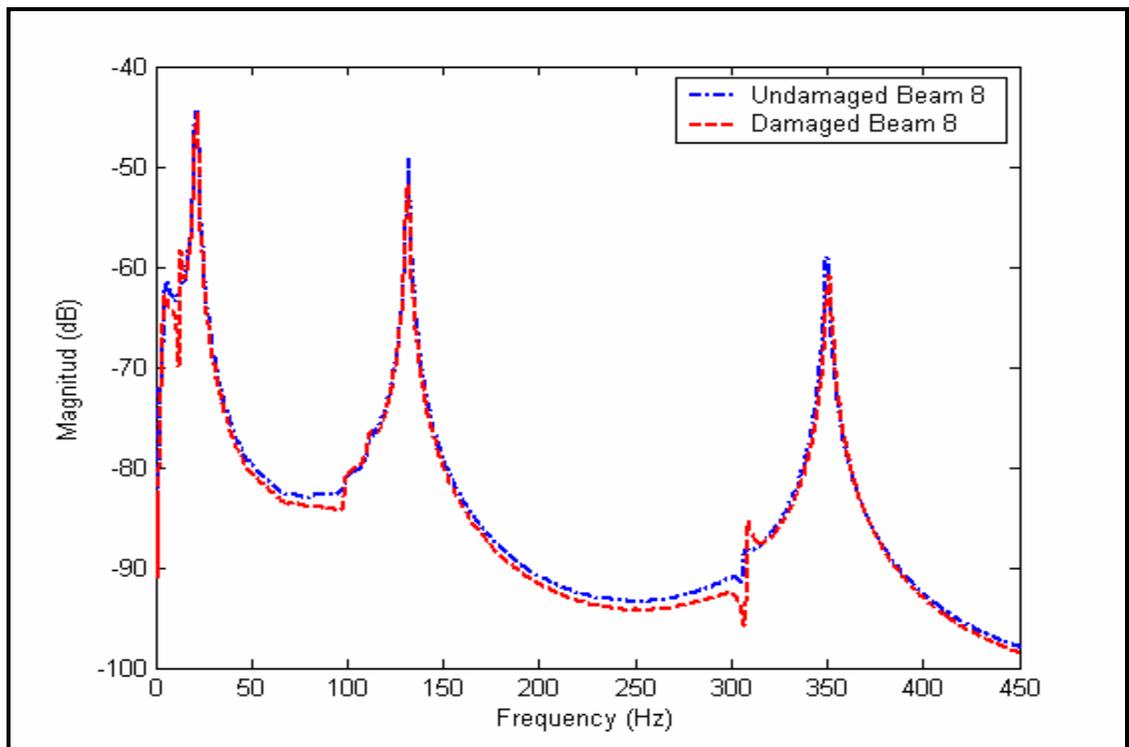


**Figure 6.9: Beam 8 - Experimental Data for Undamaged and Damaged Conditions.**

**Table 6.6: Results for Damaged Beam 8.**

| Natural Frequencies (Hz) | Experimental Data | Reduced Mass Model | Error (%) | Lumped Mass Model | Error (%) |
|---|---|---|---|---|---|
| 1$^{st}$ Natural Frequency | 21.473 | 21.48 | 0.03 | 21.473 | 0.00 |
| 2$^{nd}$ Natural Frequency | 131.520 | 131.952 | 0.33 | 132.34 | 0.62 |
| 3$^{rd}$ Natural Frequency | 350.644 | 352.609 | 0.56 | 359.294 | 2.47 |

As seen in the preceding figures the models are capable to accurately predict the dynamic behavior of the beams under study. Both models practically coincide with the experimental data for the first and second natural frequencies. For these two natural frequencies the error ranged in between 0.00 to 1.08 % with and average error of 0.29 %. Errors between the models and the experimental data for the third natural frequency were larger, the largest error being 8.19 %. These errors could be the result of a higher interaction between the modes as the frequencies increase, making the process of estimating the mode shapes from the frequency response plots more difficult. In addition, errors from torsion effects in the structure and their associated displacements along the beam help to create these discrepancies.

Overall the reduced mass model may be considered to be the more accurate when compared with the lumped mass model. This is more evident when comparing the models at higher frequencies, where the reduced model resembles the experimental data more closely. This is so because the reduced model takes into consideration the rotational degrees of freedom of the structure. The lumped mass model only considered the translational degrees of freedom for the generation of the mass matrix. Even so the lumped mass model is comparable to the experimental data. This gives us an advantage over the reduced mass model in the sense that there is no need for a previously known approximation for the stiffness matrix. Recalling the procedure to generate the reduced

mass model, the stiffness matrix was used to reduce the system and eliminate the slave degrees of freedom.

When comparing the different *FRF's* corresponding to the undamaged and damaged cases for each beam, there is no significant change in the behavior of the structure. The damage suffered by the structures was slight and did not influence much the dynamic behavior of the structure. Damping ratios and mode shapes experienced a slight change resulting in slight different damping and stiffness matrices for the beams.

**Chapter Seven:**

**Conclusions and Recommendation**

This research has demonstrated that a finite element model can be established for a sandwich composite beam using the information obtained from *FRF* plots. Both the damping matrix and the stiffness matrix of the model can be updated using this method. The system described by these matrices was used to generate *FRF's* that resembled very closely the experimental *FRF* plots taken for each beam with an average percentage of error of 0.30 % in predicting the natural frequency.

The process of generating these systems was a product of a series of steps. Because the material under study was a composite beam, no material properties were available. Prior to being able to generate the mass and stiffness matrices for a finite element model, some of the physical properties of the beams had to be estimated. Some of the properties were measured easily, but to measure the stiffness of the beam is a bit more complicated. To corroborate the accuracy of the value for the stiffness of the beam, theoretical natural frequencies were calculated and they were in accord with the experimental natural frequencies of the beams. With this estimate, it is possible to simplify the finite element model in order for it to be compatible with the available degrees of freedom. This reduction was carried out successfully through the use of an iterative procedure (*IIRS*). This reduction was programmed with the help of MATLAB software. The matrix system showed convergence for each of the beams.

The modal properties of the systems were obtained with the help of Star Modal. The software made it possible for the natural frequencies, the modal damping and the complex mode shapes of the systems to be identified. Great care must be taken when obtaining the *FRF* plots for the beams from were the modal properties were extracted. Special attention was paid to the coherence level of the *FRF's*. This value was an indication of how good the signal for the *FRF* was. A value close to one for the coherence confirmed the linearity of the system.

The models were then assembled by using an algorithm capable of identifying and updating the damping and the stiffness matrices. This algorithm used the modal

properties of the system and using an iterative procedure converged upon a damping matrix. This damping matrix was used to normalized the mode shapes of the system and successfully update the stiffness matrix. The resulting finite element model (mass, damping and stiffness matrices) was used to generate the *FRF's*, which were plotted against the experimental *FRF's*. When comparing the plots, they practically coincided with each other. From the plots, one can see that the model is fairly accurate in describing the dynamic behavior of the beams. As the number of natural frequencies increase, it is more difficult to predict the behavior of the system. This is because there is higher interaction between the modes, making it difficult to model the behavior of the system. From the plots, it is clear that the first and second natural frequencies behave almost identically to the experimental scenarios.

As far as the models are concerned, the two models developed were very similar to each other. The lumped mass model was able to represent the behavior of the system fairly accurate. This model has the advantage that it does not need an initial estimate of the stiffness of the beam in order to generate the model. The stiffness matrix for this model is completely obtained from the modal properties of the beam. In other words, we can accurately describe the behavior of the beam without knowing, beforehand, the mechanical properties of the beam.

When examining the damaged beams, there were small changes in the natural frequencies of the beam. There were also slight changes in the modal damping of each of the modes. The damaged present in the beams did not have a great effect on the stiffness of the beams. The *FRF's* for the damaged beams were compared and the represented, with accuracy, the dynamic behavior of the beams.

A methodology similar to Ortiz [3] and Pilkey [10] in formulating the damping matrix was used in this research. Natural frequency errors less than 8 percent were obtained, where as Ortiz had errors ranging up to 21 percent for a similar composite beam. Pilkey's algorithm on the other hand generated errors in the order of 8.0 percent. Both of the aforementioned methods, Ortiz's and Pilkey's, did not consider stiffness updating. In addition to the iterative damping methodology developed, this investigation used the direct formulation mentioned by Lancaster [8]. This procedure is less

computationally intensive as compared to the work by Baruch [13] and Friswell [19], which requires the use of weighted orthonormal conditions and a weighing factor chosen from user experience that is used in a penalty function, respectively.

Two models that compared the mass matrix formulation were also considered, in addition to the damping and stiffness updating. These models differed in the way the mass matrix was generated. In one method an initial guess of the stiffness of the structure is required, were as in the other a lumped mass approach was performed. The greatest error produced by these two methods when compared to the experimental *FRF* was less than 9 percent thus giving a degree of confidence in the methodology used when applied to structures similar to the one investigated. The advantage of lumped mass procedure as compared to the other is that there was no need to estimate an equivalent stiffness of the beam. This methodology makes the overall updating procedure straight forward by eliminating the use of user experience or optimization algorithms. Both models generated their greatest error in predicting higher frequency behavior which is probably due to rotational inertial effects as discussed by Friswell [23] and Humar [26].

This topic could be further investigated, by applying the methodology presented to plates. The plate has more degrees of freedom per node, and it will be interesting to prove that the iterative procedure is accurate enough to identify and update matrices for more complex structures. Other future work is the integration of this methodology to a neural network capable of distinguishing between different types of behavior of a particular structure. The neural network could learn how the model of a system is affected by different variables such as: damage magnitude and location, modal characteristics of the system, frequency shift in the *FRF* plots, dwindling of natural frequency peak due to damping change, etc. Another future work related to this topic could be a survey on the different methods for extracting modal properties, for example, damping, frequencies and mode shapes; specifically dealing with the complex behavior of structures. This survey, along with practical examples, will be very helpful when undergoing the study of structures submitted to vibration analysis.

## Bibliography

[1]  Kosmatka, J. B. and Ricles, J. M.  1999.  *Damage Detection in Structures by Modal Vibration Characterization*.  Journal of Structural Engineering, Vol. 125, No. 12: pp. 1384-1392.

[2]  Kim, J. and Ryu, Y.  1999.  *Improved Vibration-based Damage Detection Algorithm for Structures*.  Proceedings of the 17th International Modal Analysis Conference, Kissimmee: pp. 889-895.

[3]  Ortiz, Marilú.  *Vibration-Based, Non-Destructive Damping Matrix Identification for Damage Detection in a Sandwich Composite Beam*.  M. S. Thesis, University of Puerto Rico, Mayaguez, PR.

[4]  Ratcliffe, C. and Bagaria, W.  1998.  *Vibration Technique for Locating Delamination in a Composite Beam*.  AIAA Journal, Vol. 36, No. 6: pp. 1074-1077.

[5]  Tran, Danh and He, Jimin.  1998.  *Structural Damage Detection in a Simple Cantilever Plate*.  Proceedings of the 16th Modal Analysis Conference, Santa Barbara: pp. 369-373.

[6]  Wang, Z., Lin, R. M. and Lim, M. K.  1997.  *Structural Damage Detection Using Measured FRF Data*.  Computer Methods in Applied Mechanics and Engineering, Vol. 147: pp. 187-197.

[7]  Lancaster, P.  1960.  *Inversion of Lambda-Matrices and Application to the Theory of Linear Vibrations*.  Archive for Rational Mechanics and Analysis, Vol. 6: pp. 105-114.

[8]  Lancaster, P.  1961.  *Expressions for Damping Matrices in Linear Vibration Problems*.  Journal of the Aerospace Sciences: p. 256.

[9]  Pilkey, Deborah F. and Inman, D. J.  1997.  *An Iterative Approach to Viscous Damping Identification*.  Proceedings of the 15th International Modal Analysis Conference, Orlando: pp. 1152-1159.

[10] Pilkey, Deborah F.  1998.  *Computation of Damping Matrix for Finite Element Model Updating*.  Ph. D. Thesis, Virginia Polytechnic Institute and State University, Virginia.

[11] Capecchi, D. and Vestroni, F. 1999. *Monitoring of Structural Systems by Using Frequency Data*. Earthquake Engineering and Structural Dynamics, Vol. 28: pp. 447-461.

[12] Baruch, M. and Bar Itzhack, I. Y. 1978. *Optimal Weighted Orthogonalization of Measured Modes*. AIAA Journal, Vol. 16, No. 4: pp. 346-351.

[13] Baruch, M. 1978. *Optimization Procedure to Correct Stiffness and Flexibility Matrices Using Vibration Tests*. AIAA Journal, Vol. 16, No. 11: pp. 1208-1210.

[14] Ewins, D. J. 2000. *Adjustment or Updating Models*. Sādhanā, Vol. 25, Part 3: pp. 235-245.

[15] Aiad, A., Level, P. and Ravalard, Y. 1991. *A Global Updating Procedure to Improve Finite Element Models*. Université de Valenciennes, France.

[16] Imregun, M., Visser, W.J. and Ewins, D. J. 1995. *Finite Element Model Updating Using Frequency Response Function Data – I. Theory and Initial Investigation*. Mechanical Systems and Signal Processing, Vol. 9, No. 2: pp. 187-202.

[17] Friswell, M. I. and Lees, A. W. 1998. *Resonance Frequencies of Viscously Damped Structures*. Journal of Sound and Vibration, Vol. 217, No. 5: 950-959.

[18] Allemang, R. J. and Brown, D. L. 1998. *A Unified Matrix Polynomial Approach to Modal Identification*. Journal of Sound and Vibration, Vol. 211, No. 3: pp. 301-322.

[19] Friswell, M. I., Inman, D. J. and Pilkey, Deborah F. 1998. *The Direct Updating of Damping and Stiffness Matrices*. AIAA Journal, Vol. 36, No. 3: pp. 491-493.

[20] Inman, Daniel J. 1994. *Engineering Vibration*. Prentice Hall, Inc., New Jersey.

[21] Guyan, Robert J. 1965. *Reduction of Stiffness and Mass Matrices*. AIAA Journal, Vol. 3, No. 2: p. 380.

[22] O'Callahan, J. C. 1989 *A procedure for an improved reduced system (IRS) model*. Proceedings of the 7th International Modal Analysis Conference, Las Vegas.

[23] Friswell, M. I., Garvey, S. D. and Penny, J. E. T. 1998. *The Convergence of the Iterated IRS Method*. Journal of Sound and Vibration, Vol. 211, No. 1: pp. 123-132.

[24] Blevins, Robert D. 1995. *Formulas for Natural Frequency and Mode Shape*. Krieger Publishing Company, Florida.

[25] Tse, Francis S., Morse, Ivan E. and Hinkle, Rolland T. 1978. *Mechanical Vibrations: Theory and Applications*. Allyn and Bacon, Inc., Massachusetts.

[26] Humar, J. L. 1990. *Dynamics of Structures*. Prentice Hall, Inc., New Jersey.

## Appendixes

Iterated Improved Reduced System

```
% Iterative Reduction Method.
% Model is reduced in half according to
% the available data.
% Input model mass and stiffnes matrix.
format long g
K = input ('Input Stiffness Matrix ')
M = input ('Input Mass Matrix ')
[m,n] = size(K);
% Subdivision of K Matrix into 4 submatrices
% according to their relation to the master
% and slave degrees of freedom.
Kmm = K(1:m/2,1:n/2);
Kms = K(1:m/2,(n/2+1:n));
Ksm = K((m/2+1:m),1:n/2);
Kss = K((m/2+1:m),(n/2+1:n));
% Subdivision of M Matrix into 4 submatrices
% according to their relation to the master
% and slave degrees of freedom.
Mmm = M(1:m/2,1:n/2);
Mms = M(1:m/2,(n/2+1:n));
Msm = M((m/2+1:m),1:n/2);
Mss = M((m/2+1:m),(n/2+1:n));
% Subindices
% mm - master master
% ms - master slave
% sm - slave master
% ss - slave slave
t = -1*inv(Kss)*Ksm;
TS = [eye(m/2); t];
Tirs = TS;
Mr = TS'*M*TS;
Kr = TS'*K*TS;
S=[zeros(4,8); zeros(4), inv(Kss)];
```

```
i = 1;
TC = ones(8,4);
while ~isequal(TC,Tirs)
   TC = Tirs;
   Tirs = TS + S*M*Tirs*inv(Mr)*Kr;
   Mr = Tirs'*M*Tirs;
   Kr = Tirs'*K*Tirs;
   Res = Tirs - TC;
   i = i + 1;
   if i > 1000 % Iteration Control
      break
   end
end
Miirs = Tirs'*M*Tirs % Final Reduced Mass Matrix
Kiirs = Tirs'*K*Tirs % Final Reduced Stiffness Matrix
```

Iterative Procedure for Identifying and Updating the Damping and Stiffness Matrices

```
n = 4;
m = 4;
q = 4;
M = input('Mass Matrix ');
L = input ('Eigenvalues Vector ');
fi = input ('Eigenvectors Matrix ');
L = diag(L);
C0 = diag([1 1 1 1]);
C = diag([2 2 2 2]);
LSquare = L^2; % Square of Eigenvalue Matrix
a = det(C);
b = det(C0);
dd = a - b;
iter = 0;
while real(dd) > 0.000000000000001
% while iter < 25
    iter = iter + 1
    for x=1:n;
      g = 2*M*L(x,x) + C0;
        for y = 1:m;
            A(y,1) = fi(y,x);
        end
      h = transpose(A)*g*A;
      d = 1/h;
      d1 = sqrt(d);
      veca = d1*A;
        for y = 1:q
            Normvec(y,x) = veca(y,1);
        end
      normalized = Normvec;
    end
    finorm = normalized; % Normalized Eigenvectors
    conjfinorm = conj(normalized); % Conjugates of Normalized Eigenvectors
    C = C0;
```

```
     clear C0;
     a = det(C);
     C0 = -M*(finorm*LSquare*transpose(finorm) + conjfinorm*conj(LSquare)*transpose(conjfinorm))*M
     b = det(C0);
     dd = abs(a-b);
end
K = inv(-finorm*(L^-1)*transpose(finorm) - conjfinorm*(conj(L)^-1)*transpose(conjfinorm))
```

FRF Generation

## Program A

```
% FRF Generation Program.
% 4 DOF System.
% Mass matrix.
Mass = input('Mass Matrix ');;
% Damping matrix.
Damp = input('Damping Matrix ');
% Stiffness matrix.
Stiff = input('Stiffness Matrix ');
% Force vector
Bf = [1
    0
    0
    0];
% Space State System
A = [    zeros(4)         eye(4)
    -inv(Mass)*Stiff  -inv(Mass)*Damp]
B = [ zeros(4,1)
    inv(Mass)*Bf]
C = [ 0 0 0 1 0 0 0 0]
D = zeros(size(C,1),size(B,2))
sys = ss(A,B,C,D)
w = linspace(1,5000,25000);
bodemag(sys,w)
```

Program B

```
% FRF Generation Program.
% 4 DOF System.
% Mass matrix.
Mass = input('Mass Matrix ');;
% Damping matrix.
Damp = input('Damping Matrix ');
% Stiffness matrix.
Stiff = input('Stiffness Matrix ');
% Force vector
Bf = [1
    0
    0
    0];
% Space State System
A = [    zeros(4)        eye(4)
    -inv(Mass)*Stiff  -inv(Mass)*Damp]
B = [ zeros(4,1)
    inv(Mass)*Bf]
C = [ 0 0 0 1 0 0 0 0]
D = zeros(size(C,1),size(B,2))
sys = ss(A,B,C,D)
w = linspace(1,5000,25000);
bode(sys,w)
```

Plots and comparison of graphs

Example:

% Generation of graphs for composite beams experimental set up.

% Graphs represent a comparison between three models. One model uses

% the mass matrix obtained from an IIRS reduction. The second model

% uses the mass matrix generated from FEM, but only considers the

% translational degrees of freedom. The third model uses both mass

% and stiffness matrices from the FEM IIRS Model.  All slave DOF's

% and the corresponding elements in the mass matrix are not considered.

% Loading of data

load omegaHz  % Frequency Range

figure(1)

load Bar8UndMag

load Bar8LumpUndMag

load 1z5zbar8un.txt

plot    (omegaHz,Bar8UndMag,'b-.',omegaHz,Bar8LumpUndMag,'r--',X1z5zbar8un(:,1),X1z5zbar8un(:,2)-70,'k:')

legend ('Reduced Mass Model', 'Lumped Mass Model','Experimental Data')

% title ('Frequency Response Functions from Dynamic Model of Sandwich Composite Beam 5: Undamaged Scenario')

xlabel ('Frequency (Hz)')

ylabel ('Magnitud (dB)')